OFDM-Based Visible Light Communications

Chapter 12
OFDM-based Visible Light Communications

Dobroslav Tsonev, Mohamed Sufyan Islim, and Harald Haas

Abstract This chapter provides an overview of latest enhancements of the orthogonal frequency division multiplexing (OFDM) based visible light communications. The principals of OFDM techniques for intensity modulation and direct detection (IM/DD) systems are explained in details in [1]. A number of inherently unipolar OFDM techniques were recently proposed as power efficient alternatives to the widely deployed direct-current-biased optical orthogonal frequency division multiplexing (DCO-OFDM). The unipolar orthogonal frequency division multiplexing (U-OFDM) technique achieves higher power efficiency compared to DCO-OFDM. However, due to the spectral efficiency loss of U-OFDM technique, the power efficiency advantage over DCO-OFDM starts to decrease as the spectral efficiency increases. Multiple U-OFDM streams are superimposed in enhanced unipolar orthogonal frequency division multiplexing (eU-OFDM) to double the spectral efficiency of U-OFDM technique. For the first time, the novel eU-OFDM allows unipolar OFDM techniques to have same spectral efficiency of DCO-OFDM. In this chapter, the concept of eU-OFDM is generalized to GeneRalizEd ENhancEd UnipolaR OFDM (GREENER-OFDM), and extended to other unipolar OFDM schemes (asymmetrically clipped optical orthogonal frequency division multiplexing (ACO-OFDM) and pulse-amplitude-modulated discrete multitone modulation (PAM-DMT)).

12.1 Introduction

The physical properties of commercially available light emitting diodes (LEDs) and photodiodes (PDs), which are the foremost candidates for low-cost front-end devices in optical wireless communications (OWC), allow OWC to be realised as

Dobroslav Tsonev · Mohamed Sufyan Islim · Harald Haas
Li-Fi Research and Development Centre, The University of Edinburgh, Edinburgh EH9 3JL, http://www.lifi-centre.com e-mail: h.haas@ed.ac.uk

intensity modulation and direct detection (IM/DD) systems only. This is because light emitted by of-the-shelf LEDs is incoherent and so information can be reliably encoded only in the signal intensity. The phase and the amplitude of the light wave cannot be modulated or detected with LEDs and PDs. This limits the set of conventional modulation schemes that can be adopted from the field of radio frequency (RF) communications and directly translated into OWC. Signal modulation techniques such as on-off keying (OOK), pulse-position modulation (PPM), and M-ary pulse-amplitude modulation (M-PAM) are relatively straightforward to implement as they provide real signals that can be directly mapped to light intensity. However, as transmission rates increase, the limited modulation bandwidth of the front-end devices and the limited bandwidth of the OWC channel lead to intersymbol interference (ISI) in the time-domain modulation signal. Hence, a technique such as orthogonal frequency division multiplexing (OFDM) becomes more appropriate as a modulation scheme. OFDM enables simple cost-effective equalisation with single-tap equalisers in the frequency-domain. In addition, data and energy can be loaded adaptively in different frequency bands according to the channel properties. This results in an optimal exploitation of the communication resources, and it has been shown that data rates up to 100 Gbps are possible [2]. Furthermore, at a system level, OFDM provides a straightforward and low-complexity multiple access scheme, and this has to be implemented additionally for other modulation schemes such as OOK, PPM and M-PAM.

In practice, OFDM is realised in a digital signal processor (DSP) by taking an inverse fast Fourier transform (IFFT) of a block of symbols from a conventional modulation scheme such as M-ary quadrature amplitude modulation (M-QAM). This operation effectively maps the M-QAM symbols to different frequency bands of the resulting time-domain signal. However, this procedure produces complex-valued bipolar time-domain samples, while intensity modulation requires real non-negative signals. Therefore, the OFDM signal has to be modified before it becomes suitable for an IM/DD system. A real signal can be obtained by imposing Hermitian symmetry in the information block on which an IFFT operation is applied during the signal generation procedure. The resulting time-domain samples, however, would still be bipolar. A number of different approaches for obtaining a unipolar signal are given in the published research. One straightforward method is to add a bias value to all samples, which would make the resulting signal non-negative. This approach is known as direct-current-biased optical orthogonal frequency division multiplexing (DCO-OFDM). The direct current (DC) biasing leads to a significant increase in the energy consumption compared to conventional OFDM in a bipolar system. For example, a minimum bias, resulting in an energy penalty of about 6 dB compared to bipolar OFDM, is required for 4-QAM DCO-OFDM. Hence, researchers have explored alternative methods for the generation of unipolar signals. This has lead to the introduction of new inherently non-negative modulation schemes such as asymmetrically clipped optical orthogonal frequency division multiplexing (ACO-OFDM) [3] and pulse-amplitude-modulated discrete multitone modulation (PAM-DMT) [4]. These modulation techniques exploit the properties of the fast Fourier transform (FFT) and the OFDM frame structure in order to create a

symmetric time-domain signal. The negative values of these techniques waveforms can simply be reduced to zero without compromising the information in the OFDM frame. Therefore, a unipolar signal without the use of biasing can be realised. The clipping of the negative values in ACO-OFDM and M-PAM leads to an electrical energy penalty of 3 dB when compared to conventional bipolar OFDM. The scheme presented in this chapter, unipolar orthogonal frequency division multiplexing (U-OFDM), is inspired by the concept of subcarrier-index modulation orthogonal frequency division multiplexing (SIM-OFDM) and aims to close the 3 dB gap between OFDM and ACO-OFDM for bipolar signals, whilst generating a unipolar signal, which does not require biasing. It should be noted that the concepts presented for U-OFDM in the first part of this chapter have also been introduced by another research group as Flip-OFDM in [5] and in [6]. The concepts of U-OFDM and Flip-OFDM have been developed in parallel completely independently from each other and broadly within the same time period. It is interesting to note that all four approaches – ACO-OFDM, PAM-DMT, Flip-OFDM and U-OFDM – achieve the same performance in both a linear and a non-linear additive white Gaussian noise (AWGN) channel as will be illustrated later in the context of this work [3–8]. For an equivalent M-QAM/M-PAM modulation order, the spectral efficiency of each of these four methods is halved in comparison to DCO-OFDM. However, the energy penalty in comparison to a bipolar OFDM signal is only 3 dB for any M-QAM/M-PAM constellation size. Thus, the premise is that a larger constellation can be used in ACO-OFDM, PAM-DMT and U-OFDM in order to compensate for the loss in spectral efficiency from the modulation technique, but the energy efficiency can still be better than in DCO-OFDM. Improved decoders which are equivalent in performance have been developed for ACO-OFDM [9], U-OFDM [7] and Flip-OFDM [6]. Even though, to the best of the authors' knowledge, such an improved decoder is not presented in the published research for PAM-DMT, it would be straightforward to design. The improved decoders make the power efficiency of all four schemes almost equivalent to the case for a bipolar OFDM signal, but this can only work for a flat-fading communication channel. A serious problem for the inherently non-negative modulation schemes arises from the decreased spectral efficiency, which requires M-QAM DCO-OFDM to be compared to M^2-QAM ACO-OFDM/U-OFDM/Flip-OFDM and to M-PAM PAM-DMT in order to keep the achievable data rate equivalent for systems with equivalent bandwidth. This causes a substantial loss of energy efficiency compared to DCO-OFDM in all four schemes for a spectral efficiency above 1 bit/s/Hz [10]. Dissanayake *et al.* have proposed a technique to simultaneously transmit ACO-OFDM and DCO-OFDM in an attempt to close the spectral efficiency gap [11]. However, this method still requires a DC-bias for the generation of DCO-OFDM. The second part of this chapter proposes a solution to the problem of spectral efficiency loss in U-OFDM, which is extended to ACO-OFDM and PAM-DMT in a relatively straightforward fashion [12].

The rest of this chapter is organized as follows. In Sect. 12.2, the U-OFDM modulation concept is presented and then is detailed in the following subsections: in Sect. 12.2.1, the modulation and demodulation algorithm of U-OFDM is introduced; in Sect. 12.2.2, the analytical framework is presented; and in Sect. 12.2.3,

the validity of the theoretical bit error rate (BER) estimations is confirmed through extensive Monte Carlo simulations. In Sect. 12.3, an enhanced U-OFDM algorithm with an improved frame structure is proposed, this has the following subsections: in Sect. 12.3.1, the enhanced concept is presented; in Sect. 12.3.3, the analytical framework for the enhanced U-OFDM algorithm is presented; and in Sect. 12.3.4, the validity of the theoretical analysis is confirmed. In Sect. 12.4, the concept of eU-OFDM is generalized and extended to the other inherently unipolar modulation schemes, and this section is organized as follows: in Sect. 12.4.1, the concept of enhanced unipolar orthogonal frequency division multiplexing (eU-OFDM) is generalized to GeneRalizEd ENhancEd UnipolaR OFDM (GREENER-OFDM); The superposition modulation concept of eU-OFDM is extended to enhanced asymmetrically clipped optical OFDM (eACO-OFDM) in Sect. 12.4.2, and to enhanced pulse-amplitude-modulated discrete multitone modulation (ePAM-DMT) in Sect. 12.4.3; in Sect. 12.4.4, the superposition OFDM modulated techniques are compared and the optimal configurations are presented. Finally, concluding remarks are given in Sect. 12.5.

12.2 Unipolar OFDM (U-OFDM)

12.2.1 Concept

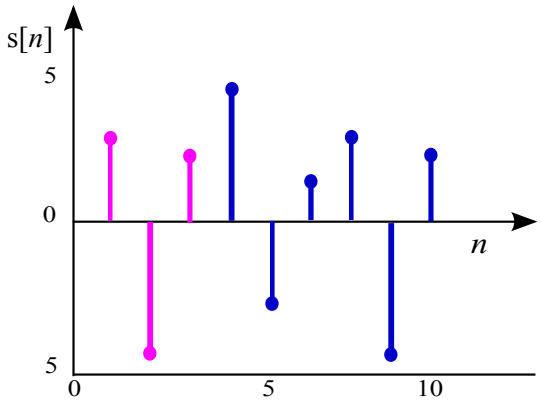

Fig. 12.1 A typical real OFDM time-domain signal. The first three samples constitute the cyclic prefix.

The U-OFDM is an algorithm for the generation of an inherently unipolar modulated signal which presents an alternative to the already familiar techniques of ACO-OFDM and PAM-DMT. The modulation process begins with the conventional generation of a real bipolar OFDM signal such as the one given in Fig. 12.1. The sign

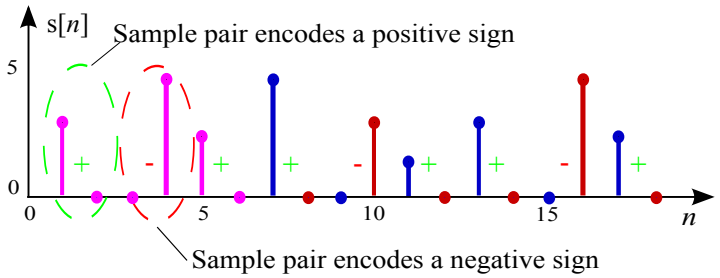

Fig. 12.2 A unipolar time-domain signal. The first six samples constitute the cyclic prefix.

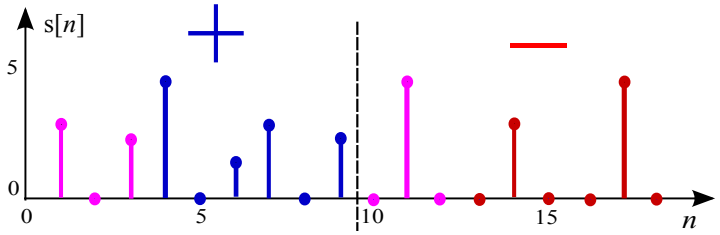

Fig. 12.3 A U-OFDM time-domain signal. The first frame contains only positive samples of the original bipolar OFDM signal. The second frame contains only negative samples of the original bipolar OFDM signal. First three samples of each frame constitute the cyclic prefix.

of a real time-domain sample amounts to exactly one bit of information. All additional information in the sample is represented by its absolute value. Absolute values are always positive. Therefore, the absolute value of a bipolar time-domain signal is a unipolar signal which can be used for transmission in IM/DD systems. Such a signal, however, has two problems. Firstly, the one-bit information for all signs has to be correctly conveyed to the destination. Secondly, the use of a non-linear transformation, such as obtaining the absolute value of a signal, creates a waveform whose frequency profile is significantly different than initially intended. This effect is very detrimental to the OFDM concept where adaptive bit and energy loading in the frequency-domain is used in order to optimise performance in a non-flat channel. A solution to the first problem can be found in [13] which introduced a very simple concept for encoding exactly one bit of information into the position of an arbitrary information symbol. Following that same approach, each time-domain sample can be encoded into a pair of new time-domain samples. If the original OFDM sample is positive, the first sample of the new pair is set as *active*, and the second sample is set as *inactive*. If, on the other hand, the original OFDM sample is negative, the first sample of the new pair is set as *inactive*, and the second sample is set as *active*. *Active* samples are set equal to the absolute value of the bipolar OFDM sample they correspond to, and *inactive* samples are set to zero. That is how the signal illustrated in Fig. 12.2 can be obtained from the signal in Fig. 12.1. Fig. 12.2 only illustrates how the signs of the bipolar samples can be encoded in the position of the *active* sample in a pair. The described operation for sign encoding is still non-linear

and changes the frequency profile of the original OFDM signal. This issue has been circumvented by an additional change in the signal structure. The actual U-OFDM signal is obtained when the first samples of each pair are grouped in their original order to form the so called *positive* block while the second samples are grouped in their original order to form the so called *negative* block. The *positive* block is transmitted first and the *negative* block is transmitted second. That is how the signal illustrated in Fig. 12.3 is obtained. This operation can also be described as the act of taking all negative samples from the original bipolar frame, replacing them with zeros and then flipping their values and transmitting them in a second frame where the positions of the original positive samples are occupied by zeros. This description of the signal generation process has given the term Flip-OFDM, used by the authors in [5]. Alternatively, the same modulation procedure can be expressed as the act of transmitting two copies of the original bipolar frame one after the other. The first copy corresponds to the *positive* block. The second copy corresponds to the *negative* block and has been multiplied by -1 in order to switch the signs of the samples. The signal is made unipolar by removing any negative values from both copies by clipping at zero. After both U-OFDM frames are received at the destination, the original bipolar frame can be recovered by subtracting the second U-OFDM frame from the first one. Afterwards, the demodulation process continues with conventional OFDM demodulation of the reconstructed bipolar signal. In the context of this work, this demodulation algorithm will be referred to as *conventional* U-OFDM demodulation. The following paragraph explains why the U-OFDM signal structure avoids the non-linearity effects from the clipping-at-zero operation.

The clipping of a signal $\mathrm{s}[n]$ at zero can be represented as:

$$\underline{\mathrm{s}}[n] = \mathrm{f}_{\mathrm{clip}}\{\mathrm{s}[n]\} = \frac{1}{2}(\mathrm{s}[n] + |\mathrm{s}[n]|). \tag{12.1}$$

If $\mathrm{s}[n]$ represents the samples of the original bipolar frame, then the transmitted samples from the first corresponding U-OFDM frame would be equal to:

$$\mathrm{s}_{\mathrm{p}}[n] = \frac{1}{2}(\mathrm{s}[n] + |\mathrm{s}[n]|). \tag{12.2}$$

The values of the second corresponding U-OFDM frame would be equal to:

$$\mathrm{s}_{\mathrm{n}}[n] = \frac{1}{2}(-\mathrm{s}[n] + |-\mathrm{s}[n]|) = \frac{1}{2}(-\mathrm{s}[n] + |\mathrm{s}[n]|). \tag{12.3}$$

After the signal is transmitted through the dispersive channel $\mathrm{h}[n]$, corrupted by AWGN, and equalized at the receiver, the respective U-OFDM frames become:

$$\hat{\mathrm{s}}_{\mathrm{E,p}}[n] = \frac{1}{2}(\mathrm{s}[n] + |\mathrm{s}[n]|) + \mathrm{n}_1[n] * \mathrm{h}^{-1}[n] \tag{12.4}$$

and

$$\hat{\mathrm{s}}_{\mathrm{E,n}}[n] = \frac{1}{2}(-\mathrm{s}[n] + |\mathrm{s}[n]|) + \mathrm{n}_2[n] * \mathrm{h}^{-1}[n], \tag{12.5}$$

where $*$ denotes the convolution operator; $\mathrm{h}^{-1}[n]$ is the inverse of the dispersive channel $\mathrm{h}[n]$; $\mathrm{n}_1[n]$ and $\mathrm{n}_2[n]$ are AWGN realisations at the receiver. The reconstructed original bipolar frame then becomes:

$$\begin{aligned}\hat{\mathrm{s}}_{\mathrm{E}}[n] = \hat{\mathrm{s}}_{\mathrm{E,p}}[n] - \hat{\mathrm{s}}_{\mathrm{E,n}}[n] = \frac{1}{2}(\mathrm{s}[n] + |\mathrm{s}[n]|) + \mathrm{n}_1[n] * \mathrm{h}^{-1}[n] - \\ - \frac{1}{2}(-\mathrm{s}[n] + |\mathrm{s}[n]|) - \mathrm{n}_2[n] * \mathrm{h}^{-1}[n] = \mathrm{s}[n] + (\mathrm{n}_1[n] - \mathrm{n}_2[n]) * \mathrm{h}^{-1}[n].\end{aligned} \tag{12.6}$$

The reconstructed signal, $\hat{\mathrm{s}}_{\mathrm{E}}[n]$, consists of the original signal, $\mathrm{s}[n]$, and a Gaussian noise component which is coloured according to the inverted frequency profile of the channel $\mathrm{h}[n]$. Despite the time-domain representation of (12.4) – (12.6), it should be noted that the equalisation step does not need to be performed in the time-domain. The subtraction step can also be performed either in the time-domain or the frequency-domain, but a time-domain operation would be the preferred choice as it would halve the number of required FFT operations. Therefore, the most cost effective sequence of demodulation steps would be subtraction → FFT → equalisation. Two observations should be made regarding the U-OFDM signal. First, the clipping term $|\mathrm{s}[n]|$ is common for both U-OFDM frames and is completely removed by the subtraction operation. Any frequency components outside the desired spectrum resulting from the clipping operation would be contained in that component. Hence, the spectrum of the estimated bipolar signal $\hat{\mathrm{s}}[n]$ would not be adversely affected by the clipping operation. Second, the noise realisations from both U-OFDM frames are combined leading to a signal-to-noise ratio (SNR) penalty of 3 dB compared to conventional bipolar OFDM transmission.

Since U-OFDM employs two frames to transmit the same information as conventional OFDM, the spectral efficiency of U-OFDM:

$$\eta_{\mathrm{U}} = \frac{\eta_{\mathrm{DCO}}}{2} = \frac{\log_2(M)(N_{\mathrm{FFT}} - 2)}{4(N_{\mathrm{FFT}} + N_{\mathrm{cp}})} \text{ bits/s/Hz}, \tag{12.7}$$

is half the spectral efficiency of DCO-OFDM, and roughly the same as the spectral efficiency of ACO-OFDM. It should be noted that this is true when the FFT size for all three modulation schemes is the same. Then U-OFDM has double the initial latency to decode a single information frame because two consecutive frames need to be received in order for the demodulation process to begin. The authors in [5] have made the case that Flip-OFDM/U-OFDM is computationally more efficient than ACO-OFDM as it requires a smaller FFT size for decoding the same information per frame. This is true for the case when the two U-OFDM/Flip-OFDM frames have a combined length equal to one ACO-OFDM frame. Then the information latency in both schemes would be the same. However, in that case, since the FFT size of U-OFDM/Flip-OFDM is half the FFT size of ACO-OFDM, the overhead of the cyclic prefix is doubled. This means that the spectral efficiency of U-OFDM/Flip-OFDM would be less than the spectral efficiency of ACO-OFDM.

For a large number of practical scenarios, when the cyclic prefix length is small, this does not introduce a significant difference. However, it would lead to a significant decrease of U-OFDM/Flip-OFDM throughput in high-speed communication scenarios, when the cyclic prefix length is expected to constitute a large portion of the frame length. Therefore, if equal spectral efficiency between ACO-OFDM and U-OFDM/Flip-OFDM is assumed for an arbitrary communication scenario, computational efficiency of U-OFDM/Flip-OFDM over ACO-OFDM cannot be claimed.

As described, the subtraction operation in the demodulation process of U-OFDM causes the noise in each pair of U-OFDM frames to combine leading to a 3-dB SNR penalty. An alternative demodulation method can be proposed in an attempt to reduce the SNR penalty. Each pair of samples, as illustrated in Fig. 12.2, encodes the amplitude and the sign of the original bipolar sample. In the same way, the value of each *active* sample in Fig. 12.3 encodes the absolute value of the original bipolar OFDM sample while its position encodes the sign. If the receiver is able to detect which is the *active* sample at each position of the U-OFDM frames, it can successfully identify the original sign and simply discard the *inactive* sample since it carries no further information, just noise. This procedure is ideally expected to remove half of the AWGN variance from the reconstructed bipolar signal in comparison to the decoder employing a subtraction operation, and, thus, it is expected to improve the performance. A simple and efficient way to identify the *active* sample is by comparing the amplitudes of the two samples at each position in a pair of U-OFDM frames, and the sample with the higher amplitude is marked as *active*. After reconstruction of the bipolar signal, the demodulation process continues with conventional OFDM demodulation. In the context of this work, this decoding scheme will be referred to as the *improved* U-OFDM decoder. A similar approach for ACO-OFDM demodulation has been reported by Asadzadeh et. al. in [9], leading to the equivalent improvement in performance, as illustrated in this work. It would be fairly straightforward to design the same decoding scheme for PAM-DMT as well, following the logic used in [9]. The *improved* decoder is only applicable in relatively flat communication channels where the ISI is negligible. If the ISI is considerable, then this demodulator requires equalisation to be performed in the time-domain. In addition, since this method discards half of the U-OFDM samples, the channel attenuation at different frequency subcarriers is not consistent. This means that the use of adaptive bit loading techniques is difficult. Furthermore, when present, low-frequency noise from ambient light flickering and the baseline wander effect in electrical circuits would further hinder the operation of the *improved* demodulation algorithm. This should be taken into account in a practical implementation. In OWC, the communication channel would often be flat, especially when a strong line-of-sight (LoS) propagation path is present. As a result, the *improved* decoder could be applied selectively, when the channel conditions are favourable, as it requires only a small modification in the processing algorithm compared to the *conventional* decoder.

12.2.2 Theoretical Bit-error-rate Analysis

This section presents a theoretical BER analysis of U-OFDM in a linear AWGN channel. The analysis of the *conventional* U-OFDM decoder is trivial as the only difference to conventional bipolar OFDM performance that needs to be taken into account is the combining of AWGN in the subtraction operation. Therefore, the theoretical BER for this demodulation scheme can be obtained by adding 3 dB to the SNR requirements of conventional bipolar OFDM for an arbitrary desired BER. The rest of this section presents the theoretical approach for analysing the performance of the *improved* demodulator for U-OFDM in an AWGN channel. In the context of the following mathematical formulas, σ_{n} is the standard deviation of the AWGN, *i.e.* , $\sigma_{\mathrm{n}} = \sqrt{BN_{\mathrm{o}}}$, where B denotes the double-sided signal bandwidth and N_{o} denotes the AWGN power spectral density (PSD); σ_{s} is the standard deviation of the real bipolar OFDM signal, $\mathrm{s}[n]$, before it is encoded in U-OFDM; $\mathrm{sgn}(s)$ is the sign function, *i.e.* ,

$$\mathrm{sgn}(s) = \begin{cases} -1 & , s < 0 \\ 0 & , s = 0 \\ 1 & , s > 0; \end{cases} \tag{12.8}$$

$\phi(x)$ is the standard normal distribution probability density function, *i.e.* ,

$$\phi(x) = \frac{1}{\sqrt{2\pi}} \mathrm{e}^{-\frac{x^2}{2}}, \tag{12.9}$$

$\mathrm{Q}(x)$ is the tail probability of the standard normal distribution, *i.e.* ,

$$\mathrm{Q}(x) = \frac{1}{\sqrt{2\pi}} \int_x^{\infty} \mathrm{e}^{-\frac{u^2}{2}} \mathrm{d}u, \tag{12.10}$$

and $\mathrm{erf}(x)$ is the error function, *i.e.* ,

$$\mathrm{erf}(x) = \frac{2}{\sqrt{\pi}} \int_0^{x} \mathrm{e}^{-u^2} \mathrm{d}u. \tag{12.11}$$

Modelling the performance of the *improved* U-OFDM decoder analytically is complicated due to the fact that during the demodulation procedure each individual sample in the time-domain is subjected to a varying non-linear transformation, which depends on two independent random variables from the AWGN. This is caused by the *active*-sample selection procedure. The distribution of a pair of received *active-inactive* samples is given in Fig. 12.4. The original *inactive* sample at the transmitter has a value of 0, so the received *inactive* sample, corrupted with AWGN from the receiver circuit, has a Gaussian distribution centred around the original value of 0. Similarly, the original *active* sample at the transmitter has a value of s, so the received *active* sample, corrupted with AWGN, has a Gaussian distribution centred around the original value of s. Let us assume that the received

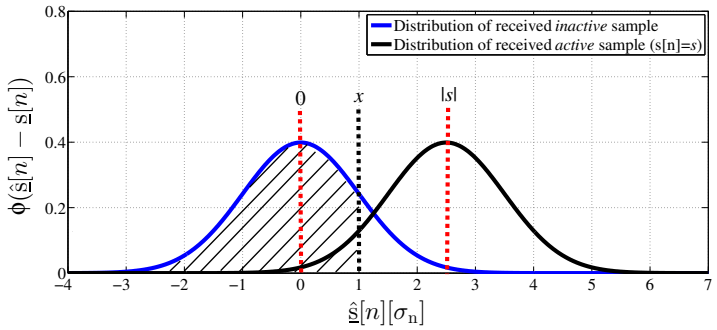

Fig. 12.4 Distribution of the received U-OFDM samples $\underline{\hat{s}}[n]$. The received U-OFDM samples are expressed in multiples of the AWGN standard deviation. The transmitted *active* sample has a value of $|s_a[n]| = |s|$ and the transmitted *inactive* sample has a value of 0. In this example, $|s| = 2.5\sigma_n$. The probability that the received *active* sample, $\underline{\hat{s}}_a[n]$, has a value of x is expressed by $1/\sigma_n \phi((x-|s|)/\sigma_n)dx$, and the probability that the received *inactive* sample, $\underline{\hat{s}}_i[n]$, has a value lower than x is denoted in the figure by the shaded area under the blue/left curve and expressed as $1-Q(x/\sigma_n)$. Similarly, the probability that $\underline{\hat{s}}_i[n]$ takes the value x is expressed by $1/\sigma_n \phi(x/\sigma_n)dx$, and the probability that $\underline{\hat{s}}_a[n]$ takes a value lower than x is denoted by the shaded area under the black/right curve and expressed as $1-Q((x-|s|)/\sigma_n)$.

active sample takes the value of x due to the AWGN. In order to *correctly* detect it as *active* at the demodulator, the value of the *inactive* sample has to take a value smaller than x. From Fig. 12.4, the probability that the *active* sample takes the value x and at the same time the *inactive* sample takes a value smaller than x is:

$$\begin{aligned} P\{\underline{\hat{s}}_a[n] = x \cap \underline{\hat{s}}_i[n] \leq x\} &= P\{\underline{\hat{s}}_a[n] = x\} P\{\underline{\hat{s}}_i[n] \leq x\} = \\ &= \frac{1}{\sigma_n}\phi\left(\frac{x-|s|}{\sigma_n}\right)\left(1 - Q\left(\frac{x}{\sigma_n}\right)\right)dx. \end{aligned} \tag{12.12}$$

This event is equivalent to the joint event of *correct* detection and the received *active* sample having a value of x. The probability of *correct* detection alone is the sum of the probabilities of all possible events $\{\underline{\hat{s}}_a[n] = x \cap \underline{\hat{s}}_i[n] \leq x\}$. Hence:

$$P\{\underline{\hat{s}}_a[n] \geq \underline{\hat{s}}_i[n]\} = \int_{-\infty}^{\infty} \frac{1}{\sigma_n}\phi\left(\frac{x-|s|}{\sigma_n}\right)\left(1 - Q\left(\frac{x}{\sigma_n}\right)\right)dx = \frac{1}{2} + \frac{1}{2}\text{erf}\left(\frac{|s|}{2\sigma_n}\right). \tag{12.13}$$

The probability that the *active* sample has the value x, given that it has been *correctly* detected, is:

$$\mathrm{P}\left\{\hat{\underline{\mathrm{s}}}_{\mathrm{a}}[n]=x|\hat{\underline{\mathrm{s}}}_{\mathrm{a}}[n]\geq\hat{\underline{\mathrm{s}}}_{\mathrm{i}}[n]\right\}=\frac{\mathrm{P}\{\hat{\underline{\mathrm{s}}}_{\mathrm{a}}[n]=x\cap\hat{\underline{\mathrm{s}}}_{\mathrm{i}}[n]\leq x\}}{\mathrm{P}\{\hat{\underline{\mathrm{s}}}_{\mathrm{a}}[n]\geq\hat{\underline{\mathrm{s}}}_{\mathrm{i}}[n]\}}=$$
$$=\frac{\frac{1}{\sigma_{\mathrm{n}}}\phi\left(\frac{x-|s|}{\sigma_{\mathrm{n}}}\right)\left(1-\mathrm{Q}\left(\frac{x}{\sigma_{\mathrm{n}}}\right)\right)}{\int_{-\infty}^{\infty}\frac{1}{\sigma_{\mathrm{n}}}\phi\left(\frac{u-|s|}{\sigma_{\mathrm{n}}}\right)\left(1-\mathrm{Q}\left(\frac{u}{\sigma_{\mathrm{n}}}\right)\right)\mathrm{d}u}\mathrm{d}x=\frac{\frac{1}{\sigma_{\mathrm{n}}}\phi\left(\frac{x-|s|}{\sigma_{\mathrm{n}}}\right)\left(1-\mathrm{Q}\left(\frac{x}{\sigma_{\mathrm{n}}}\right)\right)}{\frac{1}{2}+\frac{1}{2}\mathrm{erf}\left(\frac{|s|}{2\sigma_{\mathrm{n}}}\right)}\mathrm{d}x. \tag{12.14}$$

Therefore, (12.14) provides the probability that the original bipolar OFDM sample, $\mathrm{s}[n]=s$, is mapped to $\mathrm{sgn}(s)x$ at the receiver when *correct* detection of the *active* sample occurs. This mapping is not deterministic and varies due to the AWGN at the receiver, even when the same pair of *active* and *inactive* samples is transmitted. In order to create a more deterministic view of the transformation which each original bipolar sample undergoes in the event of *correct* detection, it can be assumed that each bipolar sample is mapped to the mean of $\mathrm{sgn}(s)x$ plus an additional noise component which represents the variation around that mean. The mean of $\mathrm{sgn}(s)x$ can be calculated as:

$$\mathrm{f_c}(s)=\int_{-\infty}^{\infty}\mathrm{sgn}(s)x\frac{\frac{1}{\sigma_{\mathrm{n}}}\phi\left(\frac{x-|s|}{\sigma_{\mathrm{n}}}\right)\left(1-\mathrm{Q}\left(\frac{x}{\sigma_{\mathrm{n}}}\right)\right)}{\int_{-\infty}^{\infty}\frac{1}{\sigma_{\mathrm{n}}}\phi\left(\frac{u-|s|}{\sigma_{\mathrm{n}}}\right)\left(1-\mathrm{Q}\left(\frac{u}{\sigma_{\mathrm{n}}}\right)\right)\mathrm{d}u}\mathrm{d}x=$$
$$=\frac{s-\mathrm{sgn}(s)\int_{-\infty}^{\infty}\frac{x}{\sigma_{\mathrm{n}}}\phi\left(\frac{x-|s|}{\sigma_{\mathrm{n}}}\right)\mathrm{Q}\left(\frac{x}{\sigma_{\mathrm{n}}}\right)\mathrm{d}x}{\frac{1}{2}+\frac{1}{2}\mathrm{erf}\left(\frac{|s|}{2\sigma_{\mathrm{n}}}\right)}=$$
$$=\frac{s-\mathrm{sgn}(s)\left(|s|\left(\frac{1}{2}-\frac{1}{2}\mathrm{erf}\left(\frac{|s|}{2\sigma_n}\right)\right)-\frac{\sigma_{\mathrm{n}}}{2\sqrt{\pi}}\mathrm{e}^{-\frac{s^2}{4\sigma_{\mathrm{n}}^2}}+\right)}{\frac{1}{2}+\frac{1}{2}\mathrm{erf}\left(\frac{|s|}{2\sigma_{\mathrm{n}}}\right)}. \tag{12.15}$$

The variance of the noise component can be calculated as:

$$\mathrm{v_c}(s)=\int_{-\infty}^{\infty}x^2\frac{\frac{1}{\sigma_{\mathrm{n}}}\phi\left(\frac{x-|s|}{\sigma_{\mathrm{n}}}\right)\left(1-\mathrm{Q}\left(\frac{x}{\sigma_{\mathrm{n}}}\right)\right)}{\int_{-\infty}^{\infty}\frac{1}{\sigma_{\mathrm{n}}}\phi\left(\frac{u-|s|}{\sigma_{\mathrm{n}}}\right)\left(1-\mathrm{Q}\left(\frac{u}{\sigma_{\mathrm{n}}}\right)\right)\mathrm{d}u}\mathrm{d}x-\mathrm{f_c^2}(s)=$$
$$=\frac{\int_{-\infty}^{\infty}\frac{x^2}{\sigma_{\mathrm{n}}}\phi\left(\frac{x-|s|}{\sigma_{\mathrm{n}}}\right)\left(1-\mathrm{Q}\left(\frac{x}{\sigma_{\mathrm{n}}}\right)\right)\mathrm{d}x}{\frac{1}{2}+\frac{1}{2}\mathrm{erf}\left(\frac{|s|}{2\sigma_{\mathrm{n}}}\right)}-\mathrm{f_c^2}(s)=$$
$$=\frac{\frac{\sigma_{\mathrm{n}}^2+s^2}{2}\left(1+\mathrm{erf}\left(\frac{|s|}{2\sigma_{\mathrm{n}}}\right)\right)+\frac{3}{4}\frac{|s|}{\sqrt{\pi}}\sigma_{\mathrm{n}}\mathrm{e}^{-\frac{s^2}{4\sigma_{\mathrm{n}}^2}}}{\frac{1}{2}+\frac{1}{2}\mathrm{erf}\left(\frac{|s|}{2\sigma_{\mathrm{n}}}\right)}-\mathrm{f_c^2}(s). \tag{12.16}$$

The communication channel is assumed to be flat when the *improved* decoder is employed. As a result, the original bipolar OFDM frame can be loaded evenly in the frequency-domain, which means that its time-domain samples can be approx-

imated by independent identically distributed (i.i.d.) Gaussian random variables when the FFT size is greater or equal to 64, $N_{\text{FFT}} \geq 64$, due to the central limit theorem (CLT) [14]. Due to the flat channel, the received U-OFDM samples would not experience any dependence in time either. At the same time, the AWGN components at each time instance are also independent. Hence, the realisations of the noise component described in (12.16) are independent from each other. As a result, due to the CLT, the noise component is transformed into an AWGN component by the FFT operation in the demodulator. The noise variance is preserved from the time-domain, and the noise mean value reflects only on the DC subcarrier which is not used for communication.

Following the reasoning described so far and the description in Fig. 12.4, the probability that the *inactive* sample takes the value x and at the same time the *active* sample takes a value smaller than x, *i.e.* , the *inactive* sample is misinterpreted as *active*, is:

$$\begin{aligned} \mathrm{P}\{\hat{\underline{\mathrm{s}}}_{\mathrm{i}}[n] = x \cap \hat{\underline{\mathrm{s}}}_{\mathrm{a}}[n] < x\} &= \mathrm{P}\{\hat{\underline{\mathrm{s}}}_{\mathrm{i}}[n] = x\}\mathrm{P}\{\hat{\underline{\mathrm{s}}}_{\mathrm{a}}[n] < x\} = \\ &= \frac{1}{\sigma_{\mathrm{n}}}\phi\left(\frac{x}{\sigma_{\mathrm{n}}}\right)\left(1 - \mathrm{Q}\left(\frac{x-|s|}{\sigma_{\mathrm{n}}}\right)\right)\mathrm{d}x \end{aligned} \tag{12.17}$$

Hence the probability of *incorrect* detection alone is the sum of the probabilities of all possible events is $\{\hat{\underline{\mathrm{s}}}_{\mathrm{i}}[n] = x \cap \hat{\underline{\mathrm{s}}}_{\mathrm{a}}[n] < x\}$, we can write:

$$\mathrm{P}\{\hat{\underline{\mathrm{s}}}_{\mathrm{a}}[n] < \hat{\underline{\mathrm{s}}}_{\mathrm{i}}[n]\} = \int_{-\infty}^{\infty} \frac{1}{\sigma_{\mathrm{n}}}\phi\left(\frac{x}{\sigma_{\mathrm{n}}}\right)\left(1 - \mathrm{Q}\left(\frac{x-|s|}{\sigma_{\mathrm{n}}}\right)\right)\mathrm{d}x = \frac{1}{2} - \frac{1}{2}\mathrm{erf}\left(\frac{|s|}{2\sigma_{\mathrm{n}}}\right). \tag{12.18}$$

Alternatively, this probability can be expressed as $1 - \mathrm{P}\{\hat{\underline{\mathrm{s}}}_{\mathrm{a}}[n] \geq \hat{\underline{\mathrm{s}}}_{\mathrm{i}}[n]\}$. The probability that the *inactive* sample has the value x, given that it has been *incorrectly* detected as *active*, is:

$$\begin{aligned} &\mathrm{P}\left\{\hat{\underline{\mathrm{s}}}_{\mathrm{i}}[n] = x | \hat{\underline{\mathrm{s}}}_{\mathrm{a}}[n] < \hat{\underline{\mathrm{s}}}_{\mathrm{i}}[n]\right\} = \frac{\mathrm{P}\{\hat{\underline{\mathrm{s}}}_{\mathrm{i}}[n] = x \cap \hat{\underline{\mathrm{s}}}_{\mathrm{a}}[n] < x\}}{\mathrm{P}\{\hat{\underline{\mathrm{s}}}_{\mathrm{a}}[n] < \hat{\underline{\mathrm{s}}}_{\mathrm{i}}[n]\}} = \\ &= \frac{\frac{1}{\sigma_{\mathrm{n}}}\phi\left(\frac{x}{\sigma_{\mathrm{n}}}\right)\left(1 - \mathrm{Q}\left(\frac{x-|s|}{\sigma_{\mathrm{n}}}\right)\right)}{\int_{-\infty}^{\infty}\frac{1}{\sigma_{\mathrm{n}}}\phi\left(\frac{u}{\sigma_{\mathrm{n}}}\right)\left(1 - \mathrm{Q}\left(\frac{u-|s|}{\sigma_{\mathrm{n}}}\right)\right)\mathrm{d}u}\mathrm{d}x = \frac{\frac{1}{\sigma_{\mathrm{n}}}\phi\left(\frac{x}{\sigma_{\mathrm{n}}}\right)\left(1 - \mathrm{Q}\left(\frac{x-|s|}{\sigma_{\mathrm{n}}}\right)\right)}{\frac{1}{2} - \frac{1}{2}\mathrm{erf}\left(\frac{|s|}{2\sigma_{\mathrm{n}}}\right)}\mathrm{d}x. \end{aligned} \tag{12.19}$$

Therefore, (12.19) provides the probability that the original bipolar OFDM sample, $\mathrm{s}[n] = s$, is mapped to $-\mathrm{sgn}(s)x$ at the receiver when the *inactive* sample is *incorrectly* detected as *active*. This mapping is not deterministic and varies due to the AWGN at the receiver, even when the same pair of *active* and *inactive* samples is transmitted. In order to create a more deterministic view of the transformation which each original bipolar sample undergoes in the event of incorrect detection, it can be assumed that the bipolar sample is mapped to the mean of $-\mathrm{sgn}(s)x$ plus an additional noise component which represents the variation around that mean. The

mean of $-\mathrm{sgn}(s)x$ can be calculated as:

$$\begin{aligned}
\mathrm{f_w}(s) &= \int_{-\infty}^{\infty} -\mathrm{sgn}(s)x \frac{\frac{1}{\sigma_\mathrm{n}}\phi\left(\frac{x}{\sigma_\mathrm{n}}\right)\left(1-\mathrm{Q}\left(\frac{x-|s|}{\sigma_\mathrm{n}}\right)\right)}{\int_{-\infty}^{\infty}\frac{1}{\sigma_\mathrm{n}}\phi\left(\frac{u}{\sigma_\mathrm{n}}\right)\left(1-\mathrm{Q}\left(\frac{u-|s|}{\sigma_\mathrm{n}}\right)\right)\mathrm{d}u}\mathrm{d}x = \\
&= \frac{\mathrm{sgn}(s)\int_{-\infty}^{\infty}\frac{x}{\sigma_\mathrm{n}}\phi\left(\frac{x}{\sigma_\mathrm{n}}\right)\mathrm{Q}\left(\frac{x-|s|}{\sigma_\mathrm{n}}\right)\mathrm{d}x}{\frac{1}{2}-\frac{1}{2}\mathrm{erf}\left(\frac{|s|}{2\sigma_\mathrm{n}}\right)} = \\
&= -\frac{\mathrm{sgn}(s)\frac{\sigma_\mathrm{n}}{2\sqrt{\pi}}\mathrm{e}^{-\frac{s^2}{4\sigma^2}}}{\frac{1}{2}-\frac{1}{2}\mathrm{erf}\left(\frac{|s|}{2\sigma_\mathrm{n}}\right)}.
\end{aligned} \tag{12.20}$$

The variance of the noise component can be calculated as:

$$\begin{aligned}
\mathrm{v_w}(s) &= \int_{-\infty}^{\infty} x^2 \frac{\frac{1}{\sigma_\mathrm{n}}\phi\left(\frac{x}{\sigma_\mathrm{n}}\right)\left(1-\mathrm{Q}\left(\frac{x-|s|}{\sigma_\mathrm{n}}\right)\right)}{\int_{-\infty}^{\infty}\frac{1}{\sigma_\mathrm{n}}\phi\left(\frac{u}{\sigma_\mathrm{n}}\right)\left(1-\mathrm{Q}\left(\frac{u-|s|}{\sigma_\mathrm{n}}\right)\right)\mathrm{d}u}\mathrm{d}x - \mathrm{f_w^2}(s) = \\
&= \frac{\int_{-\infty}^{\infty}\frac{x^2}{\sigma_\mathrm{n}}\phi\left(\frac{x}{\sigma_\mathrm{n}}\right)\left(1-\mathrm{Q}\left(\frac{x-|s|}{\sigma_\mathrm{n}}\right)\right)\mathrm{d}x}{\frac{1}{2}-\frac{1}{2}\mathrm{erf}\left(\frac{|s|}{2\sigma_\mathrm{n}}\right)} - \mathrm{f_w^2}(s) = \\
&= \frac{\frac{\sigma_\mathrm{n}^2}{2}+\frac{|s|}{4\sqrt{\pi}}\sigma_\mathrm{n}\mathrm{e}^{-\frac{s^2}{4\sigma_\mathrm{n}^2}}-\frac{\sigma_\mathrm{n}^2}{2}\mathrm{erf}\left(\frac{|s|}{2\sigma_\mathrm{n}}\right)}{\frac{1}{2}+\frac{1}{2}\mathrm{erf}\left(\frac{|s|}{2\sigma_\mathrm{n}}\right)} - \mathrm{f_w^2}(s).
\end{aligned} \tag{12.21}$$

As in the case for *correct* distinction between the *active* and *inactive* sample, the noise component in the case for *incorrect* detection is transformed into an AWGN component in the frequency-domain by the FFT operation at the demodulator.

According to the Bussgang theorem, introduced in [15], a zero-mean Gaussian random variable, X, subjected to a non-linear transformation, $\mathrm{z}(X)$, has the following properties:

$$\mathrm{z}(X) = \alpha X + Y_\mathrm{n} \tag{12.22}$$

$$\mathrm{E}\{XY_\mathrm{n}\} = 0 \tag{12.23}$$

$$\alpha = \mathrm{const.} \tag{12.24}$$

Based on these properties, the constant α and the variance of the noise Y_n can be calculated for the two separate cases of *correct* and *incorrect* detection of the *active* and *inactive* samples. In the case for *correct* detection, the original bipolar sample, $s[n]$, is mapped to $\mathrm{f_c}(s)$. In that case, the variance of Y_n and α can be calculated as:

$$\alpha_{\mathrm{c}} = \frac{\mathrm{E}\{s\mathrm{f_c}(s)\}}{\sigma_{\mathrm{s}}^2} = \frac{\int_{-\infty}^{\infty} s\mathrm{f_c}(s)\frac{1}{\sigma_{\mathrm{s}}}\phi\left(\frac{s}{\sigma_{\mathrm{s}}}\right)\mathrm{d}s}{\sigma_{\mathrm{s}}^2} \tag{12.25}$$

$$\begin{aligned} y_{\mathrm{c}} &= \mathrm{E}\{Y_{\mathrm{n,c}}^2\} - \mathrm{E}\{Y_{\mathrm{n,c}}\}^2 = \mathrm{E}\{\mathrm{f_c}^2(s)\} - \alpha_{\mathrm{c}}^2\sigma_{\mathrm{s}}^2 - \mathrm{E}\{\mathrm{f_c}(s)\}^2 = \\ &= \mathrm{E}\{\mathrm{f_c}^2(s)\} - \alpha_{\mathrm{c}}^2\sigma_{\mathrm{s}}^2 = \int_{-\infty}^{\infty} \mathrm{f_c}^2(s)\frac{1}{\sigma_{\mathrm{s}}}\phi\left(\frac{s}{\sigma_{\mathrm{s}}}\right)\mathrm{d}s - \alpha_{\mathrm{c}}^2\sigma_{\mathrm{s}}^2. \end{aligned} \tag{12.26}$$

It is apparent from (12.15) that $\mathrm{f_c}(s)$ is an odd function, so its mean in (12.26) is zero. In the case for *incorrect* detection of the *active* and *inactive* samples, the variance of Y_{n} and α can be calculated as:

$$\alpha_{\mathrm{w}} = \frac{\mathrm{E}\{s\mathrm{f_w}(s)\}}{\sigma_{\mathrm{s}}^2} = \frac{\int_{-\infty}^{\infty} s\mathrm{f_w}(s)\frac{1}{\sigma_{\mathrm{s}}}\phi\left(\frac{s}{\sigma_{\mathrm{s}}}\right)\mathrm{d}s}{\sigma_{\mathrm{s}}^2} \tag{12.27}$$

$$\begin{aligned} y_{\mathrm{w}} &= \mathrm{E}\{Y_{\mathrm{n,w}}^2\} - \mathrm{E}\{Y_{\mathrm{n,w}}\}^2 = \mathrm{E}\{\mathrm{f_w}^2(s)\} - \alpha_{\mathrm{w}}^2\sigma_{\mathrm{s}}^2 - \mathrm{E}\{\mathrm{f_w}(s)\}^2 = \\ &= \mathrm{E}\{\mathrm{f_w}^2(s)\} - \alpha_{\mathrm{w}}^2\sigma_{\mathrm{s}}^2 = \int_{-\infty}^{\infty} \mathrm{f_w}^2(s)\frac{1}{\sigma_{\mathrm{s}}}\phi\left(\frac{s}{\sigma_{\mathrm{s}}}\right)\mathrm{d}s - \alpha_{\mathrm{w}}^2\sigma_{\mathrm{s}}^2. \end{aligned} \tag{12.28}$$

It is apparent from (12.20) that $\mathrm{f_w}(s)$ is an odd function, so its mean in (12.28) is zero. The noise component Y_{n} is not correlated with the signal, according to the Bussgang theorem. At the same time, the detection events at each *active-inactive* sample pair are independent as well. Consequently, Y_{n} is transformed by the FFT operation at the demodulator into AWGN and its variance adds to the variance of the AWGN in the frequency-domain.

The variances in (12.16) and (12.21) are given as functions of s, the realisation of the signal $s[n]$. On average, over the entire duration of the OFDM frame they are equal to:

$$\bar{v}_{\mathrm{c}} = \int_{-\infty}^{\infty} \mathrm{v_c}(s)\frac{1}{\sigma_{\mathrm{s}}}\phi\left(\frac{s}{\sigma_{\mathrm{s}}}\right)\mathrm{d}s \tag{12.29}$$

and

$$\bar{v}_{\mathrm{w}} = \int_{-\infty}^{\infty} \mathrm{v_w}(s)\frac{1}{\sigma_{\mathrm{s}}}\phi\left(\frac{s}{\sigma_{\mathrm{s}}}\right)\mathrm{d}s. \tag{12.30}$$

Using (12.13), the average probability for *correct* detection of an *active* time sample, d_{c}, is:

$$d_{\mathrm{c}} = \int_{-\infty}^{\infty} \frac{1}{\sigma_{\mathrm{s}}}\phi\left(\frac{s}{\sigma_{\mathrm{s}}}\right)\left(\frac{1}{2} + \frac{1}{2}\mathrm{erf}\left(\frac{|s|}{2\sigma_{\mathrm{n}}}\right)\right)\mathrm{d}s. \tag{12.31}$$

For a large number of samples in a U-OFDM frame, the number of *correctly* and *incorrectly* detected *active* samples will have a ratio which corresponds to the prob-

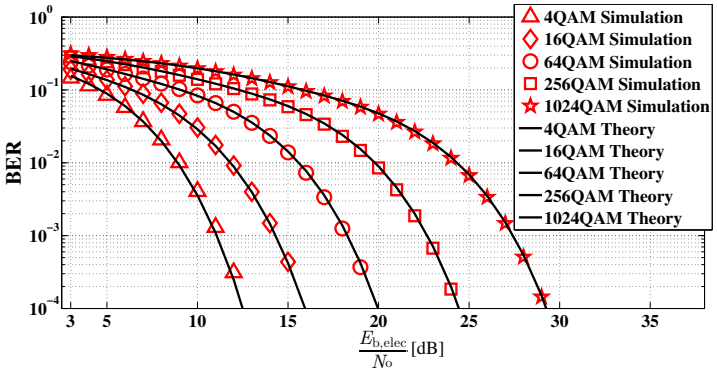

Fig. 12.5 Theoretical U-OFDM performance vs. Monte Carlo simulations

abilities for *correct* and *incorrect* detection – d_c and $1-d_c$, respectively. Hence, the average gain factor, $\bar{\alpha}$, and the average noise variance in frequency-domain, $\bar{N}$, become:

$$\bar{\alpha} = d_c \alpha_c + (1-d_c)\alpha_w \tag{12.32}$$

$$\bar{N} = d_c(\bar{v}_c + y_c) + (1-d_c)(\bar{v}_w + y_w) \tag{12.33}$$

The achieved average electrical signal-to-noise ratio ($\mathrm{SNR}_{\mathrm{elec}}$) can be plugged in the well-known formula for the BER of M-QAM [16]. Hence, the performance of U-OFDM is calculated as:

$$\mathrm{BER}_{\mathrm{U}} = \mathrm{BER}_{\mathrm{MQAM}}\left(M, \frac{\alpha^2 E_{\mathrm{b,elec}}}{\bar{N}}\right) \tag{12.34}$$

The comparison between theoretical model and Monte Carlo simulations of the system performance is presented in Fig. 12.5. There is close agreement between the presented model and the conducted simulations.

The ratio between the achieved optical signal-to-noise ratio ($\mathrm{SNR}_{\mathrm{opt}}$), and the achieved electrical SNR ($\mathrm{SNR}_{\mathrm{elec}}$) can be expressed as the ratio between the average optical power, $P_{\mathrm{opt}}^{\mathrm{avg}}$, and the average electrical power, $P_{\mathrm{elec}}^{\mathrm{avg}}$. Half of the U-OFDM time-domain samples are equal to zero and the other half follow a clipped Gaussian distribution. Hence, using the statistics of the clipped Gaussian distribution [14], the ratio between the optical power and the electrical power of the signal can be expressed as:

$$\alpha_{\mathrm{o-e}} = \frac{P_{\mathrm{opt}}^{\mathrm{avg}}}{P_{\mathrm{elec}}^{\mathrm{avg}}} = \frac{\phi(0)\sigma_s}{\sigma_s^2/2} = \frac{2\phi(0)}{\sigma_s}. \tag{12.35}$$

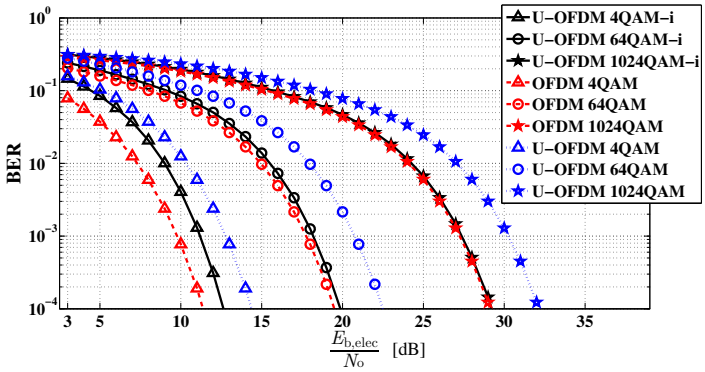

Fig. 12.6 Performance improvement introduced by the *improved* decoder for U-OFDM. The letter "i" denotes the curves for the *improved* decoder. The performance of OFDM for bipolar real signals is illustrated in this figure.

The ratio α_{o-e} can be used to obtain the equivalent SNR_{elec} for a given value of SNR_{opt}. Thus, since an analytical formula for the BER performance of the system as a function of the electrical SNR has been provided, the BER performance of the system can be evaluated analytically as a function of the optical SNR as well. This concept applies for both the *conventional* demodulation algorithm and the *improved* demodulation algorithm. For the *improved* algorithm, the BER as a function of SNR_{opt} is calculated as:

$$\text{BER}_{\text{U}} = \text{BER}_{\text{MQAM}}\left(M, \frac{\alpha^2 \alpha_{o-e} E_{b,opt}}{\bar{N}}\right). \tag{12.36}$$

12.2.3 Results and Discussion

In this section the performance of U-OFDM in a linear AWGN channel is evaluated. The AWGN channel is a good approximation of the OWC channel for the system scenarios considered in this work. Any frequency-dependent channel effects as well as non-linear distortion effects are specific for a particular system realisation and a particular deployment scenario. Therefore, they are not included in the analysis, and the linear AWGN channel is adopted as an appropriate fundamental scenario for the evaluation of the performance of U-OFDM. Furthermore, in this section, a comparison is made between the performance of the conventional DCO-OFDM scheme and the performance of U-OFDM. Since it is practically impossible to avoid clipping effects from below in DCO-OFDM due to the high peak-to-average power ratio (PAPR) of the OFDM signal, clipping of any negative values in DCO-OFDM is the only non-linear distortion adopted in this study.

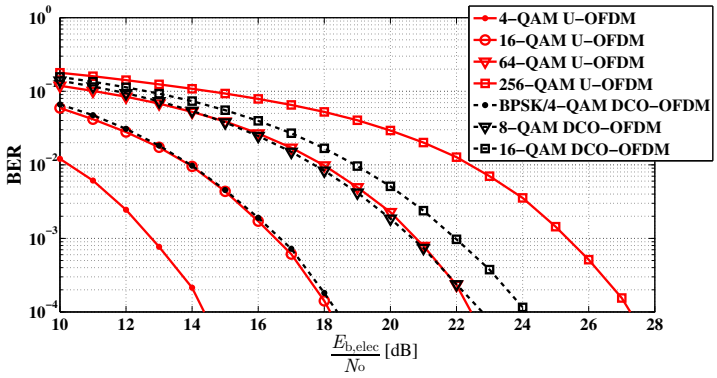

Fig. 12.7 Performance of the *conventional* decoder for U-OFDM in comparison to the performance of DCO-OFDM. The presented BER curves are generated as a function of the electrical SNR. The biasing levels for BPSK/4-QAM, 8-QAM, and 16-QAM DCO-OFDM have been set to 6 dB, 7 dB and 7.5 dB.

The *improved* U-OFDM decoder is aimed at closing the 3 dB gap between the performance of a bipolar OFDM signal and the performance of the *conventional* U-OFDM decoder. The degree to which the *improved* decoder is able to complete the task is given in Fig. 12.6. For an M-QAM constellation size of 4, the *improved* decoder closes most of the performance gap, but is still about 1.3 dB away from the target. As the constellation size increases, the gap is reduced. For example, at $M = 64$ performance difference between bipolar OFDM and the *improved* U-OFDM is approximately 0.4 dB. For $M = 1024$, the difference is 0.1 dB. Higher constellation sizes lead on average to more energy per symbol and thus lead to more signal power per time-domain sample. This in turn, reduces the probability of errors in the sample selection process conducted in the *improved* U-OFDM decoding algorithm, and therefore increases the performance improvement relative to the *conventional* U-OFDM decoding algorithm.

The performance of the *conventional* U-OFDM decoder is compared with the performance of DCO-OFDM in Fig. 12.7 and Fig. 12.8 in terms of electrical and optical energy requirements, respectively. Note that binary phase-shift keying (BPSK) OFDM and 4-QAM OFDM perform equivalently in an AWGN channel, and as a result, BPSK DCO-OFDM and 4-QAM DCO-OFDM perform equivalently. Therefore, they are represented by a single BER curve. Also note that the biasing levels for DCO-OFDM have been optimised for BER$=[10^{-4}; 10^{-3}]$ through Monte Carlo simulations, *i.e.*, lower bias levels in any of the presented cases would lead to higher BER values, and higher bias levels would lead to an increase in the signal power without reducing the BER. In terms of electrical energy dissipation, the *conventional* U-OFDM decoder exhibits performance improvement over DCO-OFDM only in the case of 4-QAM U-OFDM versus BPSK DCO-OFDM. The improvement is approximately 4 dB. For higher constellations, U-OFDM exhibits either similar or worse performance than DCO-OFDM. It is evident that, as the constellation size increases,

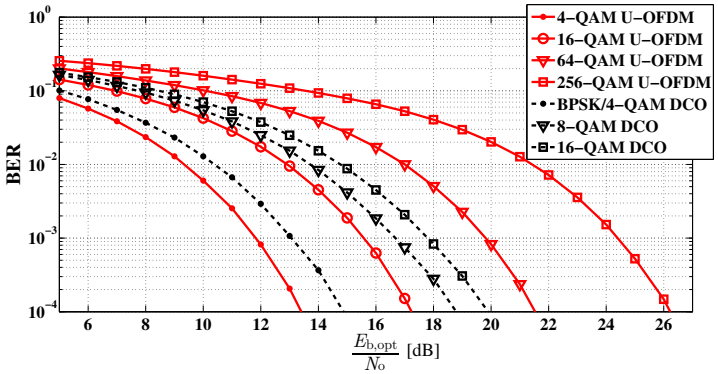

Fig. 12.8 Performance of the *conventional* decoder for U-OFDM in comparison to the performance of DCO-OFDM. The presented BER curves are generated as a function of the optical SNR. The biasing levels for BPSK/4-QAM, 8-QAM, and 16-QAM DCO-OFDM have been set to 6 dB, 7 dB and 7.5 dB.

U-OFDM requires significantly larger M-QAM constellations in order to achieve the same spectral efficiency, and, as a result, has lower performance. In terms of optical energy dissipation, U-OFDM again has an advantage over DCO-OFDM only for the case of 4-QAM U-OFDM versus BPSK DCO-OFDM, where the performance improvement is approximately 1.4 dB at a BER of 10^{-4}. For higher constellations, the optical efficiency of U-OFDM becomes worse than the efficiency of DCO-OFDM. The *improved* decoder could improve the performance of U-OFDM with up to 3 dB, as shown in Fig. 12.6. However, it is applicable only in favourable communication channel conditions as described at the end of Sect. 12.2. Furthermore, the *improved* decoder would be insufficient to compensate the electrical energy loss for U-OFDM constellation sizes larger than M=256 and the optical power loss for U-OFDM constellation sizes larger than M=16, as can be inferred from the results presented in Fig. 12.7 and Fig. 12.8, respectively. Clearly, a solution to the spectral efficiency loss in U-OFDM is required.

12.3 Enhanced Unipolar Orthogonal Frequency Division Multiplexing (U-OFDM)

The results in Sect. 12.2.3 show the great potential for energy savings introduced by a unipolar OFDM-based modulation scheme that requires no biasing. At the same time, the loss in spectral efficiency, introduced by the proposed OFDM modulation scheme, clearly diminishes the energy-saving effect of U-OFDM at low spectral efficiency and even completely eliminates any energy-saving benefit at higher spectral efficiency. Furthermore, if moderately high spectral efficiency, in the order of 4 bit/s/Hz or 5 bit/s/Hz, is required, an impractical constellation size, in the order of

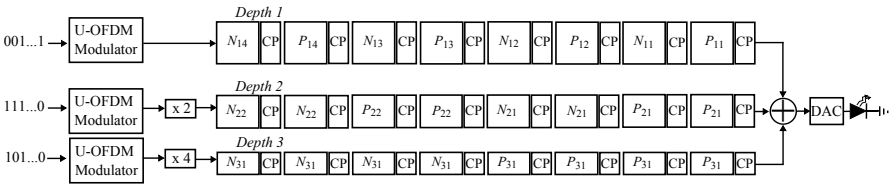

Fig. 12.9 Illustration of the enhanced U-OFDM concept up to *Depth 3*. CP denotes the individual cyclic prefix of a frame. P_{di} denotes the unipolar frame which contains the positive samples of the ith originally bipolar OFDM frame at *Depth d*. N_{di} denotes the unipolar frame which contains the absolute values of the negative samples of the ith originally bipolar OFDM frame at *Depth d*. The digital-to-analog converter (DAC) block represents the required operations, including signal amplification, for transition from a digital signal to an analog signal, capable of driving the LED front-end.

65536 or 1048576, would be necessary. Hence, in order for U-OFDM to become suitable for high-speed communication, an appropriate solution to the problem of spectral efficiency loss in the generation process has to be devised. The current section proposes an approach for solving this issue. It is referred to as enhanced unipolar orthogonal frequency division multiplexing (eU-OFDM).

12.3.1 Concept

The eU-OFDM concept is described in Fig. 12.9. The scheme combines multiple U-OFDM information streams in a single unipolar time-domain signal. All signal generation steps are performed in the digital domain and after a conventional digital-to-analog conversion, the resulting analog signal can modulate the LED without any biasing apart from the minimum requirement to turn on the LED. A single discrete U-OFDM signal in the time-domain would look exactly as the information stream at *Depth 1* in Fig. 12.9. A frame *P* contains the positive samples of an originally bipolar OFDM frame and zeros in the places of the negative samples. A frame *N* holds the absolute values of the negative samples of that same bipolar OFDM frame and zeros in the places of the positive samples. The signal at *Depth 1* is generated following the procedure described in Sect. 12.2.1. A second U-OFDM information signal, depicted at *Depth 2*, is superimposed over the signal at *Depth 1*, and it does not affect the ability of the receiver processor to separate the two signals if the following structure is followed. At *Depth 2*, each U-OFDM frame is replicated and transmitted twice, where the second frame instance is an exact copy of the first one. Hence, in Fig. 12.9, the second frame at *Depth 2* is an exact replica of the first frame, the fourth frame is an exact replica of the third frame, *etc*. This is denoted by the frame labels. Since at *Depth 2* each U-OFDM frame is transmitted twice, the amplitude of each frame instance is scaled by $\sqrt{1/2}$ in order to keep the utilised energy per bit constant. A third signal, at *Depth 3*, can be introduced similarly to the

second signal, however, the individual U-OFDM frames are replicated four times where the amplitude of each frame instance is scaled by $\sqrt{1/4}$, again in order to preserve the dissipated energy per bit. Analogously, additional information signals could be introduced, where at *Depth d*, each U-OFDM frame would be replicated into 2^{d-1} consecutive frames whose amplitude is scaled by $1/\sqrt{2^{d-1}}$.

After the information signal is received, the data signal at *Depth 1* can be demodulated straight away with the *conventional* U-OFDM decoding algorithm. Every second frame, holding the negative values of the original bipolar OFDM frame, is subtracted from its preceding frame, holding the positive values of the original bipolar OFDM frame. Then, the conventional OFDM demodulator is applied on the obtained bipolar frames. For example, at *Depth 1*, the first bipolar frame is recovered with the operation $P_{11} - N_{11}$, the second bipolar frame is recovered with the operation $P_{12} - N_{12}$ and so forth. No additional signals interfere with the successful demodulation because the interference that falls on P_{11} is equivalent to the interference that falls on N_{11}, caused by $P_{21} + P_{31}$ in the presented example. Hence, the subtraction operation cancels out both interference terms. Analogously, the interference is removed from all subsequent frames at *Depth 1*. Hence, the bits encoded at *Depth 1* can be successfully recovered with the conventional U-OFDM demodulator. Once the demodulation at *Depth 1* is complete, the demodulated bits can be remodulated again in order to recover the transmitted U-OFDM signal at *Depth 1*. This signal is then subtracted from the overall received signal, and the result contains only the information streams at *Depth 2* and above. Every two equivalent frames at *Depth 2* are summed. For example, the first and the second frame at *Depth 2* are summed, the third and the fourth frames are summed, *etc.*. Afterwards, the demodulation process continues with *conventional* U-OFDM demodulation – exactly the same way as for the recovery of the information at *Depth 1*. Again, subsequent streams do not hinder the process because the interference from all subsequent streams is structured in such a way that it is completely removed by the subtraction operation. After the bits at *Depth 2* are recovered, they are remodulated and the result is subtracted from the remaining received signal. This iterative demodulation procedure continues until the information at all depths is decoded.

12.3.2 Spectral Efficiency

The eU-OFDM scheme has increased spectral efficiency when compared to U-OFDM. The spectral efficiency of the modified scheme can be calculated as the sum of the spectral efficiencies of the different streams at all depths:

$$\eta_{\mathrm{eU}}(D) = \sum_{d=1}^{D} \frac{\eta_{\mathrm{U}}}{2^{d-1}} = \eta_{\mathrm{U}} \sum_{d=1}^{D} \frac{1}{2^{d-1}}, \tag{12.37}$$

where D is the maximum employed modulation depth in the new scheme. It equals the total number of U-OFDM streams that are superimposed in the generated mod-

Table 12.1 Spectral efficiency of eU-OFDM as a function of the maximum modulation *Depth D*.

D	1	2	3	4	5	6	7
$\frac{\eta_{\mathrm{eU}}(D)}{\eta_{\mathrm{DCO}}}$ [%]	50	75	87.5	93.75	96.88	98.44	99.22

ulation signal. As the maximum modulation depth is increased, the spectral efficiency of eU-OFDM increases, as shown in Table 12.1. For a large modulation depth, $\eta_{\mathrm{eU}}(D)$ converges to η_{DCO}, the spectral efficiency of DCO-OFDM is:

$$\lim_{D\to\infty} \eta_{\mathrm{eU}}(D) = \eta_{\mathrm{U}} \lim_{D\to\infty} \sum_{d=1}^{D} \frac{1}{2^{d-1}} = 2\eta_{\mathrm{U}} = \eta_{\mathrm{DCO}}. \tag{12.38}$$

Two practical issues should be considered at this point. First, OFDM transmission cannot start before at least a full block of bits, required for the generation of one full OFDM frame, is available at the transmitter. In real time streaming applications, this introduces a latency of at least one frame length. When eU-OFDM is used, the latency increases with the modulation depth because the binary data for at least 2^D-1 OFDM frames has to be available to the processor at the transmitter before one full eU-OFDM data block (as the one shown in Fig. 12.9) can be modulated for transmission. At the receiver side, some latency is also expected because at least 2^d frames have to be received before the demodulation at *Depth d* can be completed. Second, it can be assumed that the FFT/IFFT operation dominates the computational complexity at the receiver [5]. The eU-OFDM demodulation process requires additional FFT/IFFT operations to be performed at the receiver compared to the demodulation processes in U-OFDM and OFDM. If all subtraction procedures in the eU-OFDM demodulator are performed in the time-domain, the total number of FFT/IFFT operations is approximately double the number of FFT/IFFT operations required in OFDM because every demodulated frame has to be remodulated and, therefore, an additional IFFT operation is required. When the communication channel is not flat, this approach would introduce additional complexity in the equalisation process because the remodulated signal components would have to be distorted by the channel transfer characteristic before they are subtracted from the overall received signal. Therefore, it may be more practical if all subtraction operations in the demodulation process are performed in the frequency-domain after the FFT operation. Then, in every eU-OFDM frame, equalization has to be performed only once for the entire information signal, and no channel effects would have to be introduced to the remodulated signal. In such an implementation, however, the number of required FFT/IFFT operations is approximately four times higher than in conventional OFDM demodulation. The implementation of eU-OFDM also introduces additional memory requirements compared with OFDM because the data equivalent of 2^D OFDM frames has to be buffered for the complete demodulation of one full eU-OFDM block as shown in Fig. 12.9. The presented implementation issues put a practical limit on the highest eU-OFDM modulation depth that can be implemented with a given hardware budget. In practical applications, the hardware complexity is not expected to be problematic because for a relatively small

maximum modulation depth, the gap in spectral efficiency between eU-OFDM and DCO-OFDM is almost completely closed. For example, for D=3 and D= 5, η_{eU} is already 87.5% and 96.88% of η_{DCO}, respectively, which means the difference is practically negligible. A more detailed analysis of the eU-OFDM implementation cost is outside the scope of this work and can be addressed in future research.

12.3.3 Theoretical Bit-error-rate Analysis

12.3.3.1 Electrical Power

A real bipolar time-domain OFDM signal follows a Gaussian distribution with average electrical power of $\mathrm{E}\{\mathrm{s}^2(t)\}=\sigma_{\mathrm{s}}^2$, where σ_{s} is the standard deviation of the time-domain waveform $\mathrm{s}(t)$ [8, 17]. Therefore, half of the time-domain samples in a U-OFDM signal follow a Gaussian distribution truncated at zero, and the other half of the samples are equal to zero [7, 8]. As a result, it is straightforward to show that the average power of the time-domain U-OFDM signal is $\sigma_{\mathrm{s}}^2/2$ [7, 8]. The eU-OFDM signal is a combination of superimposed independent U-OFDM signals, and, therefore, its average time-domain electrical power grows with the number of signals that are superimposed. It can be derived as [8, 18]:

$$\begin{aligned}
P_{\mathrm{elec,eU}}^{\mathrm{avg}} &= \mathrm{E}\{\mathrm{s}_{\mathrm{eU}}^2(t)\} = \mathrm{E}\left\{\left(\sum_{d=1}^{D}\underline{\mathrm{s}}_d(t)\right)^2\right\} \\
&= \sum_{d=1}^{D}\mathrm{E}\left\{\underline{\mathrm{s}}_d^2(t)\right\} + \sum_{d_1=1}^{D}\sum_{\substack{d_2=1\\ d_1\neq d_2}}^{D}\mathrm{E}\left\{\underline{\mathrm{s}}_{d_1}(t)\right\}\mathrm{E}\left\{\underline{\mathrm{s}}_{d_2}(t)\right\} \\
&= \frac{\sigma_{\mathrm{s}}^2}{2}\sum_{d=1}^{D}\frac{1}{2^{d-1}} + \sum_{d_1=1}^{D}\sum_{\substack{d_2=1\\ d_1\neq d_2}}^{D}\frac{\phi(0)\sigma_{\mathrm{s}}}{\sqrt{2^{d_1-1}}}\frac{\phi(0)\sigma_{\mathrm{s}}}{\sqrt{2^{d_2-1}}} \\
&= \frac{\sigma_{\mathrm{s}}^2}{2}\left(2-\frac{1}{2^{D-1}}\right) + \frac{\sigma_{\mathrm{s}}^2}{2}4\phi^2(0)\sum_{d_1=1}^{D}\sum_{\substack{d_2=1\\ d_1\neq d_2}}^{D}\frac{1}{\sqrt{2^{d_1+d_2}}},
\end{aligned} \tag{12.39}$$

where $\mathrm{s}_{\mathrm{eU}}(t)$ is the eU-OFDM waveform in the time-domain; $\underline{\mathrm{s}}_d(t)$ is the U-OFDM signal at *Depth d*; and $\phi(0)$ is the probability density function (PDF) of the standard normal distribution. The time-domain expectation of the U-OFDM signal at *Depth d* is $\mathrm{E}\{\underline{\mathrm{s}}_d(t)\}=\phi(0)\sigma_{\mathrm{s}}/\sqrt{2^{d-1}}$. It is used in the calculation of (12.39) and can be derived from the statistics of the truncated Gaussian distribution described in [14]. The average number of bits that are encoded in an eU-OFDM signal is $2-1/2^{D-1}$ times more than the number of bits that are encoded in a U-OFDM signal during the same time interval. Therefore, the increase in the required SNR per bit in eU-OFDM compared with U-OFDM for the same M-QAM constellation size is the

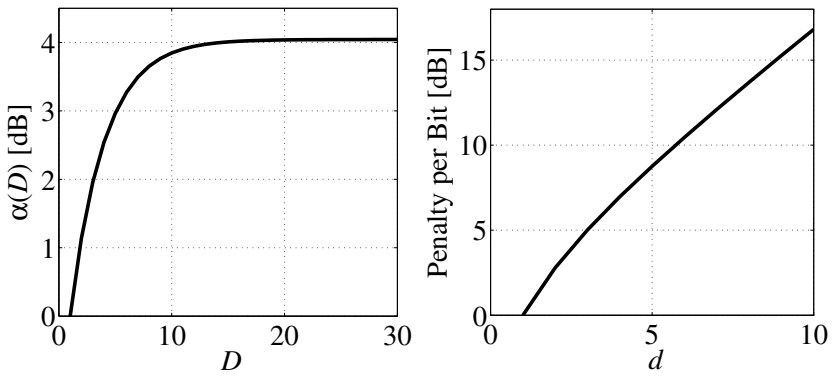

(a) Average penalty per bit as a function of the maximum modulation depth.

(b) Penalty per additional bit at a specific depth.

Fig. 12.10 Energy penalty with increasing modulation depth.

ratio of the average electrical power calculated in (12.39) and the average electrical power of the U-OFDM signal, $\sigma_s/2$, divided by the ratio of the bits encoded in the two modulation schemes, $2-1/2^{D-1}$. Hence, the increase in the required SNR for eU-OFDM is:

$$\alpha(D) = 1 + \frac{4\phi^2(0)}{2-1/2^{D-1}} \sum_{d_1=1}^{D} \sum_{\substack{d_2=1 \\ d_1 \neq d_2}}^{D} \frac{1}{\sqrt{2^{d_1+d_2}}}. \tag{12.40}$$

The electrical SNR of the system is defined as:

$$\frac{E_{\mathrm{b,elec}}}{N_\mathrm{o}} = \frac{P^{\mathrm{avg}}_{\mathrm{elec,eU}}}{B\eta_{\mathrm{eU}}N_\mathrm{o}} = \frac{\mathrm{E}\{\mathrm{s}^2_{\mathrm{eU}}(t)\}}{B\eta_{\mathrm{eU}}N_\mathrm{o}}, \tag{12.41}$$

where B is the used double-sided communication bandwidth and N_o is the double-sided PSD of the AWGN at the receiver. Fig. 10(a) shows $\alpha(D)$ for different values of the maximum modulation depth. The average SNR penalty of eU-OFDM in comparison with U-OFDM converges to about 4 dB as the spectral efficiency converges to the spectral efficiency of DCO-OFDM. As described in section 12.2.2, U-OFDM has a constant SNR penalty of 3 dB in comparison to a bipolar OFDM signal. Therefore, when this penalty is combined with the maximum penalty of about 4 dB in Fig. 10(a), it can be concluded that irrespective of the employed M-QAM constellation size, eU-OFDM has a maximum electrical SNR penalty of about 7 dB in comparison with a bipolar OFDM signal. The results in Sect. 12.2.3 indicate that DCO-OFDM has a penalty of about 7 dB in terms of electrical SNR requirements relative to a bipolar OFDM signal for BPSK and 4-QAM. Furthermore, the penalty increases when larger M-QAM constellations are used because larger constellations are more sensitive to non-linear distortion, and therefore, higher biasing levels are required

in order to reduce the clipping effect on any negative signal samples. Therefore, depending on the M-QAM constellation size used, eU-OFDM is expected to have comparable or significantly better performance than DCO-OFDM.

At this point, note the additional electrical energy per bit that is introduced at each modulation depth, d, shown in Fig. 10(b). As shown, the additional electrical energy per additional bit that is introduced when an additional U-OFDM signal is introduced to the overall information signal. The results are normalised to the energy per bit at *Depth 1*. Since the additional signals are added on top of an already existing time-domain signal, the additional electrical energy per additional bit that they introduce increases significantly with the modulation depth. This means that introducing additional U-OFDM streams to close the spectral efficiency gap between eU-OFDM and DCO-OFDM becomes inefficient in terms of energy. When the additional latency, the increased hardware complexity and the size of the spectral efficiency gap, given in Table 12.1, are also taken into consideration, it becomes evident that a practical implementation of eU-OFDM is likely to be realised for a maximum modulation depth of not more than a few streams. In case it is important that the spectral efficiency gap is closed completely, an alternative eU-OFDM implementation can be considered with different M-QAM constellation sizes at each depth. A detailed study of optimal constellation size combinations is given at Sect. 12.4.1.

A theoretical bound for the BER of eU-OFDM as a function of the electrical SNR can be estimated using the well-established formula for calculating the BER of conventional real bipolar M-QAM OFDM [16]. The only necessary modification in that formula is a scaling of the required SNR by a factor of $1/2\alpha$ to account for the 3 dB performance degradation in U-OFDM and to account for the SNR penalty incurred in eU-OFDM. The proposed theoretical bound is equivalent to the BER curve for the information stream at *Depth 1* in eU-OFDM, because in that stream any distortion is caused only by the AWGN process at the receiver since any inter-stream interference is completely removed by the subtraction operation in the demodulation procedure. The BER of the U-OFDM signals at higher depths increases with the depth because the performance is affected by the BER at lower depths. Any errors in the bit demodulation at a given depth translate into imperfections in the iterative signal cancellation algorithm. This results in reduced signal quality at all subsequent U-OFDM streams. With an increase in the SNR, the bit errors are reduced. As a result, the performance at all depths converges to the performance of the stream at *Depth 1*. This performance trend is shown in Fig. 12.11. The presented results also show very close agreement between the theoretical performance bound and the results of the Monte Carlo simulations undertaken.

12.3.3.2 Optical Power

The average optical power of the time-domain eU-OFDM signal is [8, 18]:

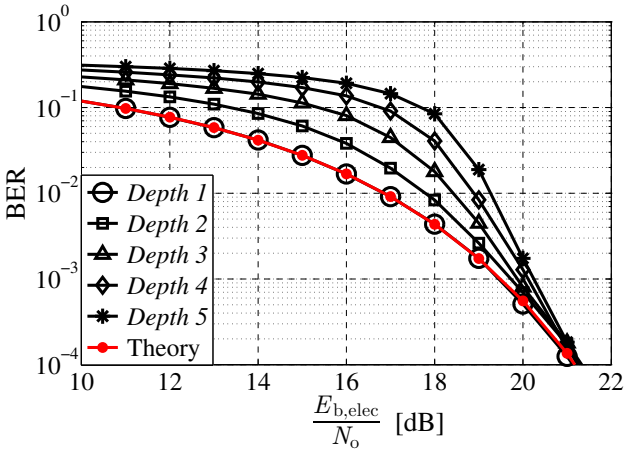

Fig. 12.11 The performance of 16-QAM eU-OFDM at different depths as a function of the electrical SNR. The curve named 'Theory' represents the theoretical performance bound.

$$P^{\mathrm{avg}}_{\mathrm{opt,eU}} = \mathrm{E}\{\mathrm{s}_{\mathrm{eU}}(t)\} = \mathrm{E}\left\{\sum_{d=1}^{D} \underline{\mathrm{s}}_d(t)\right\} = \sum_{d=1}^{D} \mathrm{E}\{\underline{\mathrm{s}}_d(t)\} \tag{12.42}$$
$$= \phi(0)\sigma_{\mathrm{s}} \sum_{d=1}^{D} \frac{1}{\sqrt{2^{d-1}}}.$$

The optical SNR of the system is defined as [8, 18]:

$$\frac{E_{\mathrm{b,opt}}}{N_{\mathrm{o}}} = \frac{P^{\mathrm{avg}}_{\mathrm{opt,eU}}}{B\eta_{\mathrm{eU}}N_{\mathrm{o}}} = \frac{\mathrm{E}\{\mathrm{s}_{\mathrm{eU}}(t)\}}{B\eta_{\mathrm{eU}}N_{\mathrm{o}}}. \tag{12.43}$$

The ratio of (12.39) and (12.42) can be used to establish a relationship between the electrical SNR and the optical SNR. Hence, for a given value of the optical SNR, the equivalent achieved electrical SNR can be calculated using this relationship. Then, the closed-form BER bound as a function of the electrical SNR can be used to establish a performance bound as a function of the optical SNR. Fig. 12.12 shows the close agreement between the proposed theoretical bound and the conducted Monte Carlo simulations. Similar to other inherently unipolar OFDM techniques, the eU-OFDM does not require a DC bias to operate. Therefore, eU-OFDM is suitable for dimmable-based visible light communications (VLC) applications. However, when illumination is desired, another arrangement for the time-domain waveform can be adopted. The PDF of the time-domain waveform can be mapped in a reversed manner so that it can achieve higher illumination levels. This can be done by:

$$\mathrm{s}^{\mathrm{rev}}_{\mathrm{eU}}(t) = I_{\mathrm{MAX}} - \mathrm{s}_{\mathrm{eU}}(t), \tag{12.44}$$

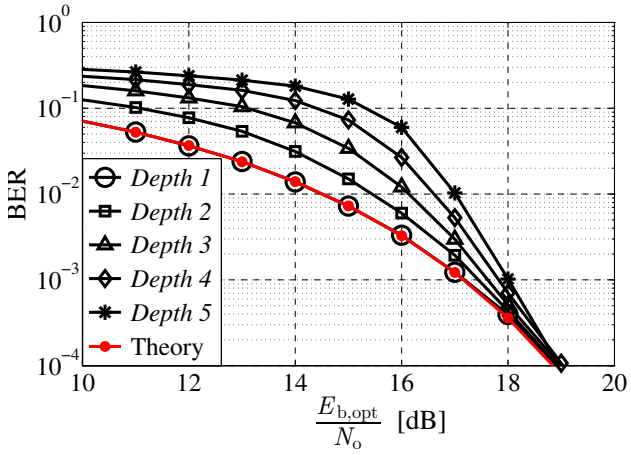

Fig. 12.12 The performance of 16-QAM eU-OFDM at different depths as a function of the optical SNR. The curve named 'Theory' represents the theoretical performance bound.

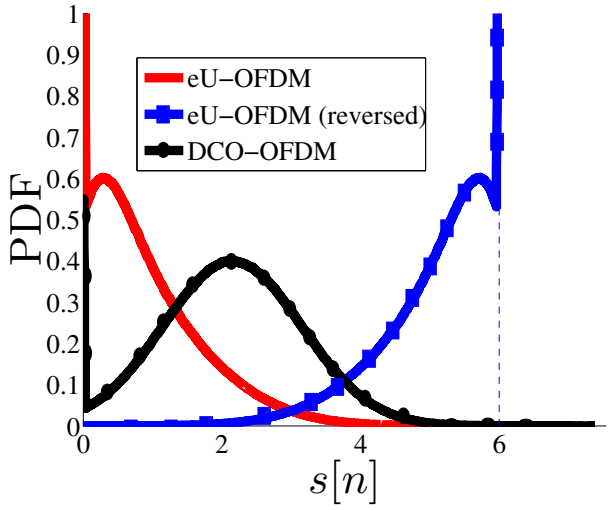

Fig. 12.13 The PDF of eU-OFDM waveform before (red curve) and after reversing (blue curve). The PDF of DCO-OFDM is also given for comparison purposes.

where I_{MAX} is the maximum allowed current of the linear region of the LED, and $s_{\mathrm{eU}}^{\mathrm{rev}}(t)$ is the reversed eU-OFDM waveform. The PDFs of eU-OFDM before and after reversing is given in Fig. 12.13. The proposed eU-OFDM can support both dimmable-based and illumination-based VLC applications in practical implementations. It should be noted that $s_{\mathrm{eU}}^{\mathrm{rev}}(t)$ would now be subject to clipping at zero level for any value of $s_{\mathrm{eU}}(t)$ higher than I_{MAX}. A more detailed analysis of this concept is outside the scope of this work and can be addressed in future research. All cal-

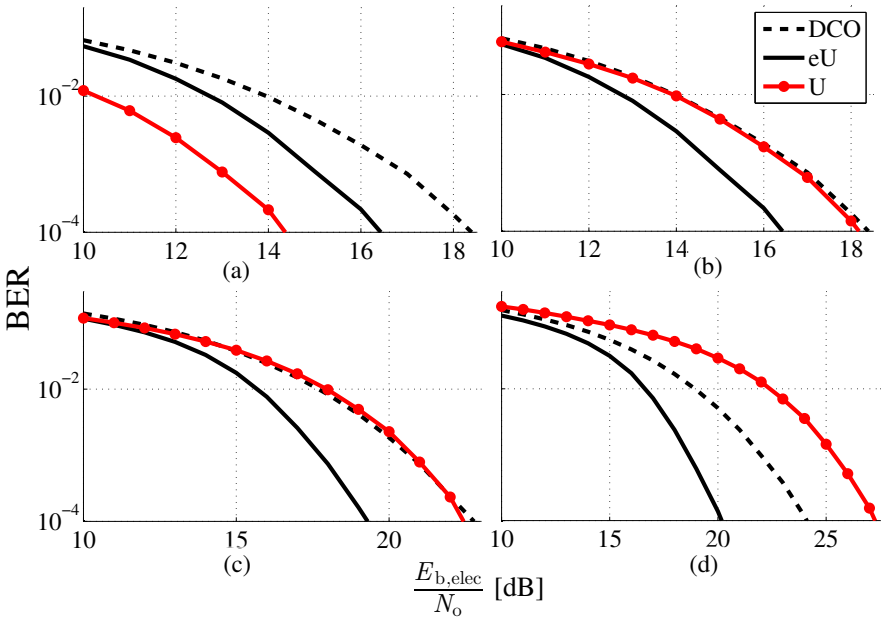

Fig. 12.14 Comparison between the performance of eU-OFDM, U-OFDM and DCO-OFDM for different M-QAM modulation orders as a function of the electrical SNR: (a) BPSK; (b) 4-QAM; (c) 8-QAM; (d) 16-QAM. The optimum bias levels for BPSK, 4-QAM, 8-QAM, and 16-QAM DCO-OFDM are estimated using Monte Carlo simulations and are set at 6 dB, 6 dB, 7 dB and 7.5 dB, respectively.

culations presented in this section are valid for an ideal front-end transmitter device under the assumption that modulation using eU-OFDM does not require biasing of the LED. However, a typical LED requires a minimum bias voltage at which the device 'turns on' and begins to emit light. In the estimation of the optical efficiency of the system, a zero bias can be assumed, because before the LED 'turns on' any light intensity output is negligible. However, when the electrical efficiency of the system is estimated, the bias should be taken into account. If the bias level is small relative to the dynamic range of the information signal, it would not introduce considerable variations in the estimated energy efficiency relative to an ideal system. Furthermore, the 'turn on' bias level is device specific. Consequently, for simplicity it is disregarded in the presented theoretical study.

12.3.4 Results and Discussion

This section presents the performance of eU-OFDM in a linear AWGN channel. As in Sect. 12.2.3, the only non-linear effect considered in this study is the effect of clipping any negative values in the information signal due to the electrical char-

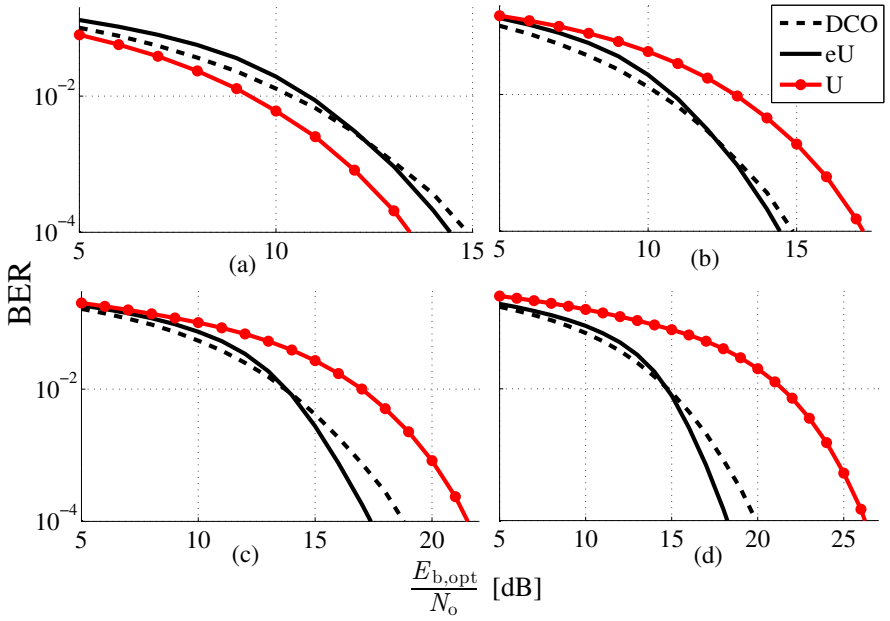

Fig. 12.15 Comparison between the performance of eU-OFDM, U-OFDM and DCO-OFDM for different M-QAM modulation orders as a function of the optical SNR: (a) BPSK; (b) 4-QAM; (c) 8-QAM; (d) 16-QAM. The optimum bias levels for BPSK, 4-QAM, 8-QAM, and 16-QAM DCO-OFDM are estimated using Monte Carlo simulations and set at 6 dB, 6 dB, 7 dB and 7.5 dB, respectively.

acteristics of an ideal LED. The simulations have been performed in a flat fading channel because the presented scheme eU-OFDM is a multicarrier technique in the same way the benchmark technique against which it is compared DCO-OFDM is a multicarrier technique. When subjected to the same communication channel, the individual subcarriers between the OFDM-based techniques are subjected to the same attenuation by the channel. As a result, the SNR penalty due to the channel in both techniques is the same. The eU-OFDM scheme generates a strictly positive signal and, therefore, it completely avoids clipping of the signal from below, whilst DCO-OFDM is subjected to this non-linear effect. In the presented study, the maximum depth of eU-OFDM is chosen to be D=3 because at this depth, the larger part of the spectral efficiency gap between DCO-OFDM and U-OFDM is closed. In addition, for this value of D, the implementation complexity is still manageable and the theoretical and simulation results provided in this section can be compared against experimental results described [19]. Therefore, in all of the results presented in this section, the spectral efficiency of eU-OFDM is actually 87.5% of the spectral efficiency of DCO-OFDM in agreement with Table 12.1.

The average BER achieved for the decoded information at all depths in eU-OFDM is compared against the BER of DCO-OFDM and U-OFDM for different M-QAM constellation sizes. Fig. 12.14 presents the BER results for constellation

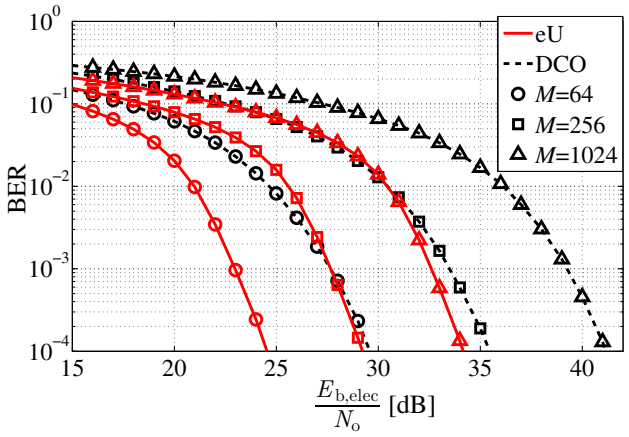

Fig. 12.16 Performance of eU-OFDM compared against the performance of DCO-OFDM for different M-QAM modulation orders as a function of the electrical SNR. The optimum bias levels for 64-QAM, 256-QAM, and 1024-QAM DCO-OFDM are estimated using Monte Carlo simulations and are set at 9.5 dB, 11 dB and 13 dB, respectively.

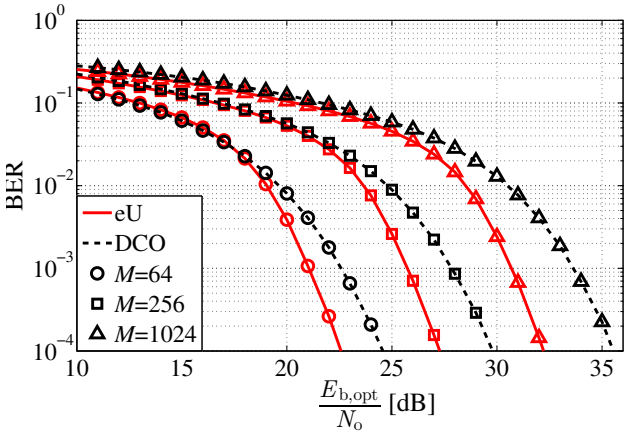

Fig. 12.17 Performance of eU-OFDM compared against the performance of DCO-OFDM for different M-QAM modulation orders as a function of the optical SNR. The optimum bias levels for 64-QAM, 256-QAM and 1024-QAM DCO-OFDM are estimated using Monte Carlo simulations and are set at 9.5 dB, 11 dB and 13 dB, respectively.

sizes $M = [2,4,8,16]$ as a function of the electrical SNR. For U-OFDM, an actual constellation size of M^2 is used for each respective value of M, so that equal spectral efficiency can be achieved by the three schemes. The results are presented for BER values down to 10^{-4} because in practice most forward error correction (FEC) codes are able to deliver reliable communication at such BERs [20]. The electrical efficiency improvement of eU-OFDM over DCO-OFDM begins at around 2 dB for BPSK and increases to about 4 dB for 16-QAM. In DCO-OFDM, the bias levels

for the different M-QAM constellations are optimised through Monte Carlo simulations and are in agreement with previous work [14, 21]. The introduced bias levels are deemed optimal because in each of the presented cases adding less bias leads to more clipping distortion and therefore to higher BER for a given SNR. At the same time, adding more bias leads to higher energy dissipation without any reduction of the BER. The bias levels are expressed as the estimated SNR increase in dB relative to a bipolar OFDM signal. In eU-OFDM, for a maximum depth of D=3, the SNR penalty is $\alpha \approx 1.95$ dB according to Fig. 10(a). This SNR penalty is constant irrespective of the constellation size. Therefore, the apparent increase in energy efficiency of eU-OFDM over DCO-OFDM with an increase in the M-QAM modulation order can be explained and quantified. Fig. 12.14 also shows the loss in energy efficiency for U-OFDM as the spectral efficiency increases. In Fig. 12.14(a), 4-QAM U-OFDM is more energy efficient than both BPSK eU-OFDM and BPSK DCO-OFDM. In Fig. 12.14(b) and 12.14(c), 16-QAM U-OFDM and 64-QAM U-OFDM are less energy efficient than 4-QAM eU-OFDM and 8-QAM eU-OFDM, respectively, while at the same time exhibiting approximately the same efficiency as 4-QAM DCO-OFDM and 8-QAM DCO-OFDM. In Fig. 12.14(d), 256-QAM U-OFDM is evidently less energy efficient than both 16-QAM eU-OFDM and 16-QAM DCO-OFDM. Fig. 12.15 presents the same performance trends in all three modulation schemes as a function of the optical SNR. For BPSK and 4-QAM, eU-OFDM exhibits an efficiency advantage of about 0.5 dB over DCO-OFDM. This optical power advantage reaches almost 2 dB for 16-QAM. At the same time, U-OFDM exhibits an advantage only for a constellation size of $M = 4$ when compared with BPSK eU-OFDM and BPSK DCO-OFDM, as given in Fig. 12.15(a).

A performance comparison between eU-OFDM and DCO-OFDM is also presented for higher spectral efficiency values. Fig. 12.16 and Fig. 12.17 show results for $M = [64, 256, 1024]$. In this study, U-OFDM is not considered because it has already been demonstrated that the scheme loses its energy advantage over both eU-OFDM and DCO-OFDM for 256-QAM U-OFDM compared with 16-QAM eU-OFDM/DCO-OFDM. The results presented in Fig. 12.16 and Fig. 12.17 show that for 1024-QAM, eU-OFDM can attain savings of approximately 7 dB in electrical energy dissipation over DCO-OFDM, and approximately 3 dB less in required optical power. Such results can make a significant difference in future high speed OWC systems.

12.4 Superposition Modulation for Orthogonal Frequency Division Multiplexing (OFDM)

An alternative arrangement of the modulation sizes used in eU-OFDM is explored in this section. The GeneRalizEd ENhancEd UnipolaR OFDM (GREENER-OFDM) allows the spectral efficiency gap of U-OFDM and DCO-OFDM to be completely closed with a maximum of three depths. The eU-OFDM concept described in this chapter is based on the unique time-domain structure in every pair of U-OFDM

frames. Analogous unique structures are also present in the other two well-known unipolar OFDM modulation schemes, ACO-OFDM and PAM-DMT. Hence, the GREENER-OFDM concept is extended to ACO-OFDM and PAM-DMT.

12.4.1 Generalized Enhanced Unipolar Orthogonal Frequency Division Multiplexing (U-OFDM)

12.4.1.1 Concept

The spectral efficiency of eU-OFDM approaches the spectral efficiency of DCO-OFDM as the maximum number of depths increases. However, implementation issues, outlined in section 12.3.2, put a practical limit on the maximum number of depths that can be used. The eU-OFDM was introduced as a special case of the GREENER-OFDM [22], where it was assumed that the constellation sizes and the power allocations are the same for all information streams. However, in order for the spectral efficiency gap between eU-OFDM and DCO-OFDM to be completely closed, an alternative setting of constellation sizes should be exploited. All possible combinations of constellation sizes at the different eU-OFDM streams with all possible power allocations are investigated in this section for a maximum number of depths $D = 3$. The modulation concept of GREENER-OFDM is similar to the modulation concept of eU-OFDM described in section 12.3.1. The only difference is that, each stream at *Depth d* is now modulated with an arbitrary modulation size M_d-QAM and scaled with an additional scaling value γ_d.

12.4.1.2 Spectral Efficiency

The spectral efficiency of the GREENER-OFDM can be expressed as the sum of the spectral efficiencies of the individual information streams:

$$\eta_{\mathrm{GO}}(D) = \sum_{d=1}^{D} \frac{\eta_{\mathrm{U}}(d)}{2^{d-1}} \quad \text{bits/s/Hz}, \tag{12.45}$$

where $\eta_{\mathrm{U}}(d)$ is the spectral efficiency of the U-OFDM streams given in (12.7) for a modulation size M_d at *depth d*. In order for the GREENER-OFDM spectral efficiency to match the spectral efficiency of DCO-OFDM, the used combination of constellation sizes should satisfy the following constraint:

$$\log_2(M_{\mathrm{DCO}}) = \sum_{d=1}^{D} \frac{\log_2(M_d)}{2^d}, \tag{12.46}$$

where M_{DCO} is the constellation size of the M_{DCO}-QAM DCO-OFDM. For example, two 16-QAM streams match the spectral efficiency of 8-QAM DCO-OFDM; or a

64-QAM stream at *Depth 1* in combination with a 16-QAM stream at *Depth 2*; or a combination of a 32-QAM stream at *Depth 1* and two subsequent 16-QAM streams at *Depth 2* and *Depth 3* is enough to achieve the same spectral efficiency as 16-QAM DCO-OFDM. The spectral efficiency ratio of the GREENER-OFDM to the U-OFDM scheme at *depth d* can be expressed as the ratio of (12.45) to (12.7):

$$\alpha_{\eta}(D,d) = \frac{\eta_{\mathrm{GO}}(D)}{\eta_{\mathrm{U}}(d)} = \frac{\sum_{\acute{d}=1}^{D}(\log_2(M_{\acute{d}})/2^{\acute{d}})}{\log_2(M_d)/2}. \tag{12.47}$$

12.4.1.3 Theoretical Bit-error-rate Analysis

The electrical average power of GREENER-OFDM can be written as [22]:

$$P_{\mathrm{elec,GO}}^{\mathrm{avg}}(D,\underline{\gamma}) = \mathrm{E}\left[\mathrm{s}_{\mathrm{GO}}^2(t)\right] = \mathrm{E}\left[\left(\sum_{d=1}^{D}\mathrm{s}_d(t)\right)^2\right]$$

$$= \sigma_{\mathrm{s}}^2\left(\sum_{d=1}^{D}\frac{\gamma_d^{-2}}{2^d} + 2\phi^2(0)\sum_{d_1=1}^{D}\sum_{\substack{d_2=1\\ d_1\neq d_2}}^{D}\frac{(\gamma_{d_1}\gamma_{d_2})^{-1}}{\sqrt{2^{d_1+d_2}}}\right), \tag{12.48}$$

where $\mathrm{s}_{\mathrm{GO}}(t)$ is the time-domain GREENER-OFDM waveform; $\mathrm{s}_d(t)$ is the time-domain U-OFDM signal at *depth d*; and $\underline{\gamma} = \{\gamma_d^{-1}; d = 1,2,\ldots,D\}$ is the set of scaling factors applied to each corresponding stream. Similarly, the average optical power for the GREENER-OFDM can be written as [22]:

$$P_{\mathrm{opt,GO}}^{\mathrm{avg}}(D,\underline{\gamma}) = \sum_{d=1}^{D}\mathrm{E}[\underline{\mathrm{s}}_d(t)] = \phi(0)\sigma_{\mathrm{s}}\sum_{d=1}^{D}\frac{\gamma_d^{-1}}{\sqrt{2^{d-1}}}, \tag{12.49}$$

The power allocation for each individual stream is optimized with respect to the average power of the modulation signal, which should satisfy the following constraints:

$$P_{\mathrm{elec,GO}}^{\mathrm{avg}}(D,\underline{\gamma}) \leq P_{\mathrm{elec,GO}}^{\mathrm{avg}}(D,\mathbf{1}_{1\times D}),$$
$$P_{\mathrm{opt,GO}}^{\mathrm{avg}}(D,\underline{\gamma}) \leq P_{\mathrm{opt,GO}}^{\mathrm{avg}}(D,\mathbf{1}_{1\times D}), \tag{12.50}$$

The electrical power penalty per bit incurred by GREENER-OFDM in comparison to U-OFDM can be written as:

$$\alpha_{\mathrm{elec}}(D,d,\underline{\gamma}) = \frac{\alpha_{\mathrm{elec}}^{P}(D,\underline{\gamma})}{\alpha_{\eta}(D,d)}, \tag{12.51}$$

where $\alpha_{\eta}(D,d)$ is given by (12.47), and $\alpha_{\mathrm{elec}}^{P}(D,\underline{\gamma})$ is the increase in average electrical power of GREENER-OFDM to the average electrical power of a scaled U-OFDM at *depth d*, $P_{\mathrm{elec,U}}^{\mathrm{avg}}(\gamma_d) = \sigma_{\mathrm{s}}^2/(2\gamma_d^2)$, which can be expressed as:

$$\alpha^{P}_{\text{elec}}(D,\underline{\gamma}) = \frac{P^{\text{avg}}_{\text{elec,GO}}(D,\underline{\gamma})}{P^{\text{avg}}_{\text{elec,U}}(\gamma_d)}. \tag{12.52}$$

A theoretical bound on the BER performance of the GREENER-OFDM information streams can be derived using the previously used formula for the BER of M-QAM [16]. A closed-form theoretical bound on the BER performance at *Depth* d, as a function of the electrical BER, can be estimated by scaling the SNR by a factor of $1/2\alpha_{\text{elec}}(D,d)$ to account for the SNR loss in U-OFDM and to account for the electrical SNR penalty in GREENER-OFDM. This can be expressed as:

$$\text{BER}^{\text{GO}}_{(D,d,\underline{\gamma})} \cong \text{BER}_{\text{MQAM}}\left(M_d, \frac{E_{\text{b,elec}}}{2N_o\alpha_{\text{elec}}(D,d,\underline{\gamma})}\right). \tag{12.53}$$

Similar to eU-OFDM, the BER performance of all streams at higher depths is affected by the BER performance of the streams at the lower depths. Therefore (12.53) is presented as a closed-form theoretical lower bound on the achievable BER. A closed-form bound on the BER performance of the overall GREENER-OFDM can be obtained by considering the spectral efficiency contribution of each individual depth given in (12.47). The overall performance bound can be expressed as:

$$\text{BER}_{\text{GO}} \cong \sum_{d=1}^{D}\left(\frac{\text{BER}^{\text{GO}}_{(D,d,\underline{\gamma})}}{\alpha_{\eta}(D,d)}\right). \tag{12.54}$$

The BER performance bound as a function of the optical SNR can be obtained by inserting the ratio of (12.49) and (12.48) into (12.53) and (12.54). The optimal combinations of constellation sizes and their corresponding scaling factors for GREENER-OFDM are obtained using both the theoretical model and Monte Carlo simulations. The optimality is defined as the lowest energy requirements among other spectrally equivalent combinations. The performance of the optimum configurations in GREENER-OFDM is compared with the performance of spectrally equivalent OFDM techniques in Sect. 12.4.4.

12.4.2 Enhanced Asymmetrically-clipped Optical OFDM (ACO-OFDM)

The symmetry in U-OFDM lies in frames, whilst in ACO-OFDM and pulse-amplitude-modulated discrete multitone modulation (PAM-DMT), it lies in subframes. In ACO-OFDM, only the odd subcarriers are modulated. As a consequence, the samples within one time-domain frame of the bipolar signal, $s[n]$, before the asymmetrical clipping have the property: $s[n] = -s[n+N_{\text{FFT}}/2]$ as shown in [3, 8]. If only the even subcarriers are modulated, the time-domain frame has the property: $s[n] = s[n+N_{\text{FFT}}/2]$ [8]. The opposite relations also hold. Therefore, as long as the

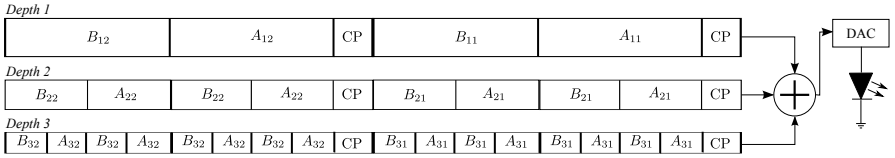

Fig. 12.18 Illustration of the enhanced ACO-OFDM. CP indicates the unique cyclic prefix of each frame. A_{dl} indicates the first half, from sample 0 to sample $N_{\text{FFT}}/2-1$, of the lth ACO-OFDM frame at *Depth* d. B_{dl} indicates the second half, from sample $N_{\text{FFT}}/2$ to sample $N_{\text{FFT}}-1$, of the lth ACO-OFDM frame at *Depth* d.

interference in the first half of the frame, from sample 0 to sample $N_{\text{FFT}}/2-1$, is equivalent to the interference in the second half of the frame, from sample $N_{\text{FFT}}/2$ to sample $N_{\text{FFT}}-1$, any distortion due to interference falls only on the even subcarriers in the frequency-domain. Hence, it is orthogonal to the information, which is modulated only on the odd subcarriers. A possible arrangement of the multiple ACO-OFDM streams is given in Fig. 12.18 [23]. The eACO-OFDM signal generation starts at the first depth with an ACO-OFDM modulator. The subframes are defined to be half of the original ACO-OFDM frames in length and they are considered to be the basis for eACO-OFDM streams. Subsequent streams are generated in a similar way to the first stream but with an OFDM frame length $N_d = N_{\text{FFT}}/2^{d-1}$. All generated frames are repeated 2^{d-1} times and scaled by a factor $1/2\gamma_d$. An arbitrary modulation size M_d-QAM is employed at each individual *Depth* d. The cyclic prefixs (CPs) are not required to be repeated as they are already included at the end of each repeated subframe. The demodulation process at the receiver would be applied in a similar fashion to the GREENER-OFDM. The information at *Depth 1* can be recovered directly as in conventional ACO-OFDM because all of the inter-stream-interference falls into the even-indexed subcarriers. After the first stream is decoded, the information can be remodulated again and subtracted from the overall signal. Then, frames which are equivalent at *Depth 2* can be recombined and the demodulation procedure can continue as for the stream at *Depth 1*. The algorithm can be applied until the information from all streams is recovered. The theoretical BER analysis of eACO-OFDM is identical to the analysis of GREENER-OFDM, therefore the optimal modulation sizes and scaling factors are the same. The performance of the optimum configurations in eACO-OFDM is presented in Sect. 12.4.4.

12.4.3 Enhanced Pulse-amplitude-modulated Discrete Multitone Modulation (PAM-DMT)

12.4.3.1 Concept

In PAM-DMT, all subcarriers are modulated with imaginary symbols from an M-PAM scheme as described in [4, 8]. If the interference over a single PAM-DMT

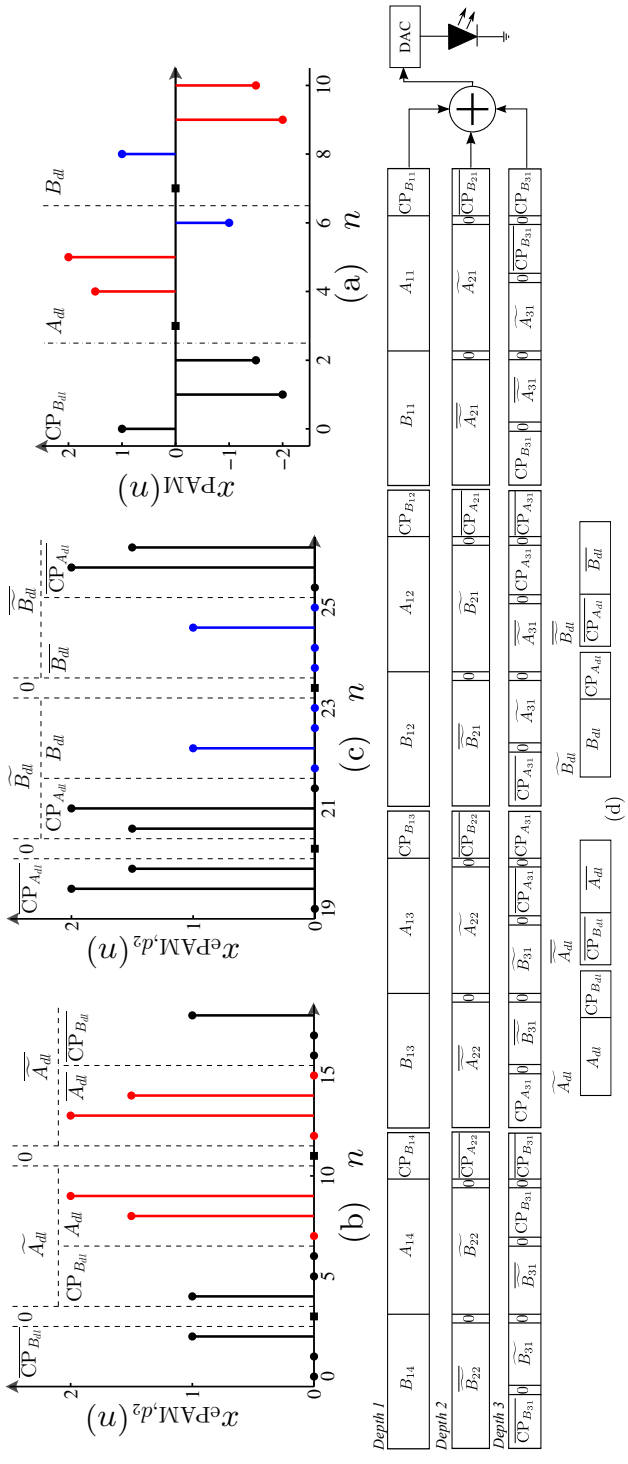

Fig. 12.19 Illustration of the ePAM-DMT. **(a)** presents the PAM-DMT time-domain waveform and its cyclic prefix before zero clipping. **(b)** and **(c)** present two unipolar ePAM-DMT frames at *Depth 2*. **(d)** presents the complete frame structure arrangement for three information streams. At any depth, the first half of the PAM-DMT frame is denoted as A_{dl}, while B_{dl} denotes the second half of the same PAM-DMT frame. The bar notation $\overline{F}$ refers that the subframe F is flipped $\overline{F}[n] = \overline{F}[N_F - 1 - n]$, where N_F is the length of F. Modified subframes $\widetilde{A}_{dl}$ and $\widetilde{B}_{dl}$ are shown in the figure alongside their flipped versions A_{dl} and B_{dl}, respectively. The subscripts denote that the frame at *Depth d* belongs to the *l*-th PAM-DMT frame.

frame duration possesses a Hermitian symmetry in the time-domain, then its frequency profile is a real signal. Hence, the interference is completely orthogonal to the useful information which is encoded in imaginary symbols. A possible arrangement of the multiple PAM-DMT streams in ePAM-DMT is given in Fig.12.19 (d) [24]. The generation process starts at *Depth 1* with a PAM-DMT modulator, where each generated frame is composed of a cyclic prefix, $\mathrm{CP}_{B_{dl}}$, and two subframes, A_{dl} and B_{dl}, where d denotes the depth index, and l denotes the frame number, as shown in Fig. 12.19 (a). The bar notation $\overline{F}$ denotes that the subframe F is flipped, $F[n] = \overline{F}[N_F - 1 - n]$, where N_F is the length of F. At *Depth 2*, the information is generated using another PAM-DMT modulator with a smaller OFDM frame length. The frame length at *Depth d* is given by: $N_d = N_{d-1} - 2N_{\mathrm{CP}} - 2$, $\forall d \geq 2$, where $N_1 = N_{\mathrm{FFT}}$. The original subframe A_{dl} is combined with the cyclic prefix $\mathrm{CP}_{B_{dl}}$ to form a modified subframe $\widetilde{A_{dl}}$. The modified subframe is flipped and repeated in $\overline{\widetilde{A_{dl}}}$. Therefore, the two modified subframes at *Depth 2*, $\widetilde{A_{dl}}$ and $\overline{\widetilde{A_{dl}}}$, each prefixed with a zero sample form a new frame that is similar in length to the previous depth frames. Moreover, these two modified subframes have a Hermitian symmetry that allows distortion-free inter-stream interference at lower depths. A cyclic prefix $\overline{\mathrm{CP}_{B_{dl}}}$ that is identical to the last N_{CP} samples of each frame is required. Therefore, frames at *Depth 2* need three cyclic prefixes. The first one is intended to guard the modified frames from ISI at the demodulation process of the first stream. The other two prefixes are intended to guard the original frames from ISI at the demodulation process of the second stream. The subsequent frames in *Depth 2* are generated in a similar way to the first frame. The time-domain waveform for the first two frames at *Depth 2* are shown in Fig. 12.19 (b) and (c). Frames at *Depth 2* are scaled by $1/\sqrt{2}$ in order to preserve the overall signal energy at this depth. At *Depth 3*, frames are generated in a similar way to *Depth 2* frames. The frame length is smaller than the previous stream frame length and the cyclic prefixes are designed to create three layers of ISI protection for each of the demodulation processes at the receiver. The information conveyed in the *Depth 3* subframes is repeated four times in a way that preserves the Hermitian symmetry for each demodulation process at higher depths. Frames at *Depth 2* are scaled by $1/2$ in order to preserve the overall signal energy at this depth. In addition, each of the streams is scaled by a parameter $1/\gamma_d$ to facilitate the optimization of the allocated power at that stream. The proposed design requires a maximum of $D = 3$ depths to achieve the spectral efficiency of DCO-OFDM, since an arbitrary modulation size M-PAM is employed at each individual *Depth d*. At the receiver, the information carried at *Depth 1* can be extracted using a PAM-DMT demodulator, since all of the inter-stream interference caused by the other streams affects the real component of the frequency subcarriers. Afterwards, the recovered bits at *Depth 1* are remodulated in order to reconstruct the stream-1 information signal, which is then subtracted from the overall received ePAM-DMT signal. Subsequently, the second half of each frame is removed from the ePAM-DMT waveform. The length of the removed subframes is $N_1/2$. Therefore the resulted waveform conveys the *Depth 2* and *Depth 3* information but with a hierarchy that is similar to *Depth 1* and *Depth 2* as shown in Fig.12.19 (d). This allows the demodulation process at higher depths to be performed in a similar way to *Depth 1*

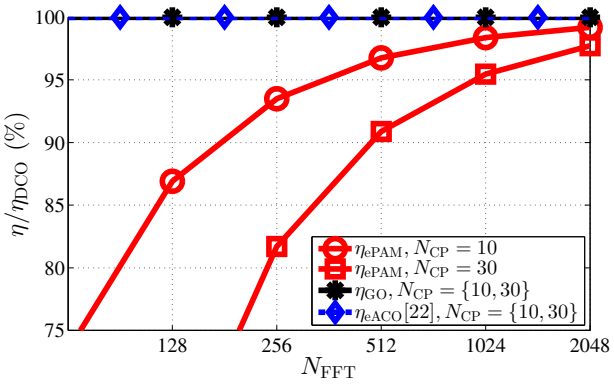

Fig. 12.20 The spectral efficiency of eACO-OFDM (η_{eACO}), ePAM-DMT (η_{ePAM}), and GREENER-OFDM (η_{GO}) compared to the spectral efficiency of DCO-OFDM (η_{DCO}), as a function of the frame length N_{FFT} and cyclic prefix length $\mathrm{N_{CP}}$. $N_{\mathrm{FFT}} = N_1$ for ePAM-DMT.

demodulation. The multiple cyclic prefixes are intended to protect the subframes at each demodulation process and are arranged to preserve the Hermitian symmetry required for this technique. The demodulation process continues in a similar way for all subsequent streams until the information at all depths is recovered.

12.4.3.2 Spectral Efficiency

The spectral efficiency of PAM-DMT at the first depth is equivalent to the spectral efficiency of DCO-OFDM for the same constellation size and the same frame length. The spectral efficiency of PAM-DMT at *Depth d* can be given by:

$$\eta_{\mathrm{PAM}}(d) = \frac{\log_2(M_d)(N_d - 2)}{2^d(N_{\mathrm{FFT}} + N_{\mathrm{CP}})} \quad \text{bits/s/Hz}, \tag{12.55}$$

where M_d and N_d are the constellation size and the OFDM frame length at *Depth d*, respectively, and $N_1 = N_{\mathrm{FFT}}$. In order to improve the power efficiency, the ePAM-DMT employs multiple streams of PAM-DMT with small constellation sizes. Therefore, the combination of constellation sizes are required to follow the constraint:

$$\log_2(M_{\mathrm{DCO}}) = 2\sum_{d=1}^{D} \frac{\log_2(M_d)}{2^d}. \tag{12.56}$$

The spectral efficiency of ePAM-DMT is given as the sum of the spectral efficiencies of the individual PAM-DMT streams. It can be written as [24]:

$$\eta_{\mathrm{ePAM}}(D) = \sum_{d=1}^{D} \eta_{\mathrm{PAM}}(d)$$

$$= \sum_{d=1}^{D} \frac{\log_2(M_d)\,(N_{\mathrm{FFT}} - 2 - 2(N_{\mathrm{CP}}+1)(d-1))}{2^d (N_{\mathrm{FFT}} + N_{\mathrm{CP}})}. \tag{12.57}$$

Since multiple cyclic prefixes are required to compact the ISI effects, the spectral efficiency of ePAM-DMT cannot match the spectral efficiency of DCO-OFDM exactly. Among all of the possible sets of constellation sizes obtained in this paper, the worst case scenario is presented in Fig. 12.20. The spectral efficiency ratio is shown as a function of the OFDM frame and cyclic prefixes lengths. Fig. 12.20 shows that $\eta_{\mathrm{ePAM}}(D)$ is higher than 90% of η_{DCO} for all of the presented cyclic prefix lengths when the frame length $N_{\mathrm{FFT}} \geq 512$. The spectral efficiency ratio of the ePAM-DMT to a PAM-DMT scheme with a similar constellation size can be expressed as:

$$\begin{aligned} \alpha_{\eta}^{\mathrm{ePAM}}(D,d) &= \frac{\eta_{\mathrm{ePAM}}(D)}{\eta_{\mathrm{PAM}}(d)} \\ &= \frac{\sum_{\acute{d}=1}^{D} \log_2(M_{\acute{d}})(N_{\acute{d}} - 2)/2^{\acute{d}}}{\log_2(M_d)(N_{\mathrm{FFT}} - 2)/2}. \end{aligned} \tag{12.58}$$

12.4.3.3 Theoretical Bit-error-rate Analysis

The PAM-DMT waveform follows a truncated Gaussian distribution [8]. Therefore, the average electrical and optical power of ePAM-DMT are similar to the average electrical and optical power of GREENER-OFDM given in (12.48) and (12.49), respectively. Therefore, the increase in the dissipated electrical energy per bit in ePAM-DMT compared with the electrical energy dissipation per bit in PAM-DMT stream at *Depth d* is given by the ratio of (12.52) and (12.58):

$$\alpha_{\mathrm{elec}}^{\mathrm{ePAM}}(D,d,\underline{\gamma}) = \frac{\alpha_{\mathrm{elec}}^{P}(D,\underline{\gamma})}{\alpha_{\eta}^{\mathrm{ePAM}}(D,d)}. \tag{12.59}$$

A theoretical bound on the BER performance of the ePAM-DMT streams is derived using the same formula for the BER performance used for the previous techniques [16]. The achieved electrical SNR at the receiver should be scaled by a factor of $1/2$ to account for the SNR loss in M-PAM, and by a factor of $1/\alpha_{\mathrm{elec}}^{\mathrm{ePAM}}(D,d)$ to account for the electrical SNR penalty in ePAM-DMT. An additional scaling factor of $1/2^{d-1}$ is required, because half of the frames are removed in the demodulation process at each depth. Although this could be avoided in AWGN channels, here it has been considered to expand the versatility of the ePAM-DMT proposed system. In addition, the corresponding constellation size should be squared since the performance of $\sqrt{M}$-PAM is equivalent to the performance of M-QAM. The theoretical bound on the BER performance of ePAM-DMT can be expressed as [23]:

$$\mathrm{BER}_{(D,d,\underline{\gamma})}^{\mathrm{ePAM}} \cong \frac{2}{\log_2(M_d)}\left(1-\frac{1}{M_d}\right) \times \sum_{l=1}^{R} \mathrm{Q}\left((2l-1)\sqrt{\frac{6E_{\mathrm{b,elec}}/N_{\mathrm{o}}\log_2(M_d)}{2^d \alpha_{\mathrm{elec}}^{\mathrm{ePAM}}(D,d)(M_d^2-1)}}\right), \tag{12.60}$$

where $E_{\mathrm{b,elec}}/N_{\mathrm{o}}$ is the electrical SNR of real bipolar OFDM, and $R = \min(2, \sqrt{M_d})$. Similar to other superposition OFDM techniques, the BER of the higher order depths is affected by the BER performance of the lower order depths. The average BER for ePAM-DMT can be derived by considering the spectral efficiency contribution of each depth. The average BER performance can then be expressed as:

$$\mathrm{BER}_{\mathrm{ePAM}} \cong \sum_{d=1}^{D} \left(\frac{\mathrm{BER}^{\mathrm{ePAM}}_{(D,d,\underline{\gamma})}}{\alpha^{\mathrm{ePAM}}_{\eta}(D,d)} \right). \tag{12.61}$$

The BER performance bound as a function of the optical SNR can be obtained by inserting the ratio of (12.49) and (12.48) into (12.60) and (12.61). The performance of ePAM-DMT is compared to the other superposition OFDM modulation techniques in Sect. 12.4.4.

12.4.4 Results and Discussion

The performance of the optimum configurations in all of the superposition modulated schemes is compared in this section with the performance of a spectrally equivalent DCO-OFDM in an AWGN channel. The optimal combinations of constellation sizes and their corresponding scaling factors for GREENER-OFDM, eACO-OFDM, and ePAM-DMT are obtained using both the theoretical model and Monte Carlo simulations and presented in Table 12.2. The simulation model is identical to the model adopted in Sect. 12.3.4. The BER performances of the superposition OFDM schemes are presented in Fig. 12.21(a) for the electrical SNR and in Fig. 12.21(b) for the optical SNR. The spectral efficiency for ePAM-DMT is higher than 97% of the spectral efficiency of DCO-OFDM. The eACO-OFDM/GREENER-OFDM performances are equivalent for all cases, since the optimal configurations used are identical. The theoretical BER values are in close agreement with the Monte Carlo results for all of the presented cases. Both GREENER-OFDM and eACO-OFDM are more energy efficient than DCO-OFDM in terms of the electrical SNR for all the presented spectral efficiencies, except at $\eta = 1$ bit/s/Hz where the BER performance is approximately equivalent to the BER of DCO-OFDM. As shown in Fig. 12.21(a), the electrical energy savings for both GREENER-OFDM and eACO-OFDM starts with 2.83 dB at $\eta = 2$ bit/s/Hz to reach 4.35 dB at $\eta = 5$ bits/s/Hz. As shown in Fig. 12.21(b), Both GREENER-OFDM and eACO-OFDM are less energy efficient than DCO-OFDM at $\eta = 1$ bit/s/Hz for the optical SNR. However, at $\eta = 2$ bits/s/Hz, both GREENER-OFDM and eACO-OFDM are more energy efficient than DCO-OFDM with 0.7 dB optical SNR savings. The BER performance of GREENER-OFDM and eACO-OFDM, as a function of the optical SNR, is approximately equivalent to the BER of DCO-OFDM for spectral efficiency values above 2 bits/s/Hz. The ePAM-DMT is less energy efficient than GREENER-OFDM and eACO-OFDM at all the presented spectral efficiency values, for both electrical and

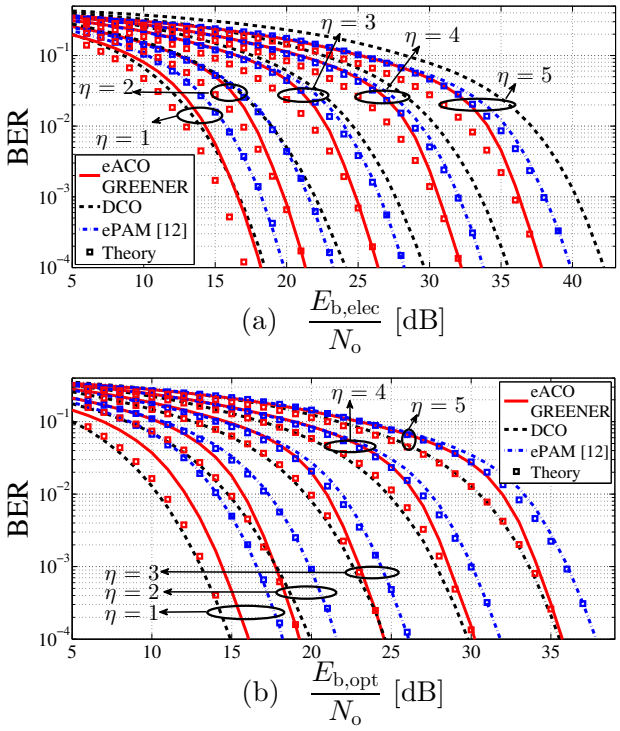

Fig. 12.21 The BER performance of eACO-OFDM versus ePAM-DMT versus GREENER-OFDM versus DCO-OFDM for different spectral efficiencies, in an AWGN channel as a function of **(a)** the electrical SNR and **(b)** the optical SNR. The value of η is given in bits/s/Hz. The optimum DC bias levels for DCO-OFDM at $\eta = \{1,2,3,4,5\}$ are estimated through Monte Carlo simulations at respectively 6 dB, 7.5 dB, 9.5 dB, 11 dB and 13 dB.

optical SNR. This is because of the 3 dB loss at each demodulation process, and because the optimal configurations for ePAM-DMT are suboptimal as the non-squared M-QAM BER performance can never be achieved using the $\sqrt{M}$-PAM modulation scheme. The ePAM-DMT is more energy efficient than DCO-OFDM in terms of the electrical SNR at spectral efficiency values above 1 bit/s/Hz. When compared with DCO-OFDM, the electrical energy savings for ePAM-DMT starts with 0.85 dB at $\eta = 2$ bits/s/Hz to reach 2.29 dB at $\eta = 5$ bits/s/Hz. In terms of the optical SNR, the ePAM-DMT is less energy efficient than DCO-OFDM for all of the presented values. The optical energy loss of ePAM-DMT compared with DCO-OFDM is 3.25 dB at $\eta = 1$; 1.6 dB at $\eta = 2$; 1.48 dB at $\eta = 3$; 2 dB at $\eta = 3$; and 2.29 dB at $\eta = 5$ where η is given in bits/s/Hz. Higher optical energy dissipation is a desirable property for illumination based VLC applications. However, it is considered as a disadvantage for dimmable-based VLC applications.

Table 12.2 The optimal combination of constellation sizes and scaling factors for enhanced ACO-OFDM and GREENER-OFDM where M_d and γ_d denote the constellation size and the scaling factor for the modulation *Depth d*, respectively.

DCO-OFDM	GREENER-OFDM/eACO-OFDM		η
M_{DCO}-QAM	$\{M_1, M_2, ..., M_D\}$-QAM	$\underline{\gamma}$ [dB]	[bit/s/Hz]
2-QAM	{2,4}-QAM	{2.2,-2.4}	0.5
4-QAM	{8,2,4}-QAM	{-2.3,5.9,1.4}	1
8-QAM	{16,8,4}-QAM	{-1.8,1.4,5}	1.5
16-QAM	{32,16,16}-QAM	{-1.4,1.7,2}	2
32-QAM	{64,64,16}-QAM	{-0.9,-0.7,5.3}	2.5
64-QAM	{128,128,64}-QAM	{0,-0.4,2.6}	3
128-QAM	{256,256,256}-QAM	{0,0,0}	3.5
256-QAM	{512,1024,256}-QAM	{0.5,-2.2,3.8}	4
512-QAM	{2048,1024,256}-QAM	{-1.9,1.1,6.8}	4.5
1024-QAM	{4096,2048,1024}-QAM	{-1.7,1.4,4.3}	5

Table 12.3 The optimal combination of constellation sizes and scaling factors for enhanced PAM-DMT, where M_d and γ_d denote the constellation size and the scaling factor for the modulation *Depth d*, respectively.

DCO-OFDM	ePAM-DMT		η
M_{DCO}-QAM	$\{M_1, M_2, ..., M_D\}$-PAM	$\underline{\gamma}$ [dB]	[bit/s/Hz]
2-QAM	-	-	0.5
4-QAM	{2,4}-PAM	{5.2,-4}	1
8-QAM	{4,4}-PAM	{1.1,-1.4}	1.5
16-QAM	{8,4}-PAM	{-1,2.2}	2
32-QAM	{8,8,4}-PAM	{0.7,-1.7,1.5}	2.5
64-QAM	{16,8,4}-PAM	{-1.7,1.3,4.5}	3
128-QAM	{32,8,4}-PAM	{-3,5.6,8.8}	3.5
256-QAM	{32,16,16}-PAM	{-0.8,2,-0.5}	4
512-QAM	{64,16,16}-PAM	{-2.6,5.9,3.2}	4.5
1024-QAM	{64,64,16}-PAM	{0.2,-2.4,6.3}	5

12.5 Conclusions and Future Directions

A novel modulation approach for the generation of energy efficient unipolar OFDM signals, termed U-OFDM, has been introduced in this chapter. The scheme offers significant energy savings in terms of electrical energy consumption and optical power requirements when compared with the conventional DCO-OFDM. All benefits, however, come at a 50% reduction in the scheme spectral efficiency. When equal spectral efficiency is assumed, U-OFDM outperforms DCO-OFDM only for relatively small M-QAM constellation sizes. A modified approach, termed eU-OFDM, has been proposed as a solution to the spectral efficiency reduction problem in U-OFDM. Using eU-OFDM, the spectral efficiency gap between U-OFDM and DCO-OFDM is almost closed, and significant power savings are attained. The superposition concept of eU-OFDM is generalized in GREENER-OFDM, and extended to other unipolar OFDM techniques in eACO-OFDM and ePAM-DMT.

The problem of spectral efficiency loss has been a long-standing issue in the inherently unipolar state-of-the-art techniques including ACO-OFDM, PAM-DMT and the novel U-OFDM. The solutions proposed in this chapter exploits the OFDM frame structure in a novel way and allows multiple information streams to be transmitted simultaneously. The novel concept effectively introduces a new degree of freedom in the signal space of U-OFDM, ACO-OFDM and PAM-DMT. For the first time, the spectral efficiency of DCO-OFDM has been matched by an inherently unipolar OFDM-based modulation scheme which does not require an increase in the M-QAM modulation order and still attains manageable implementation complexity and also significant energy benefits. Future research on this topic should analyse the front-end devices nonlinearity effects on the system performance.

Acknowledgements The authors acknowledges support from the EPSRC under grants EP/K008757/1 and EP/K00042X/1.

References

1. Dimitrov S, Haas H (2015) Principles of LED Light Communications: Towards Networked Li-Fi. Cambridge University Press
2. Tsonev D, Videv S, Haas H (2015) Towards a 100 Gb/s Visible Light Wireless Access Network. Opt Express 23(2):1627–1637, doi: 10.1364/OE.23.001627, http://www.opticsexpress.org/abstract.cfm?URI=oe-23-2-1627
3. Armstrong J, Lowery A (2006) Power Efficient Optical OFDM. Electronics Letters 42(6):370–372, doi: 10.1049/el:20063636
4. Lee SCJ, Randel S, Breyer F, Koonen AMJ (2009) PAM-DMT for Intensity-Modulated and Direct-Detection Optical Communication Systems. IEEE Photonics Technology Letters 21(23):1749–1751, doi: 10.1109/LPT.2009. 2032663
5. Fernando N, Hong Y, Viterbo E (2011) Flip-OFDMfor Optical Wireless Communications. In: Information Theory Workshop (ITW), IEEE, IEEE, Paraty, Brazil, pp 5–9, doi: 10.1109/ITW.2011.6089566
6. Fernando N, Hong Y, Viterbo E (2012) Flip-OFDM for Unipolar Communication Systems. IEEE Transactions on Communications 60(12):3726–3733, doi: 10.1109/TCOMM.2012.082712.110812
7. Tsonev D, Sinanovic S, Haas H (2012) Novel Unipolar Orthogonal Frequency DivisionMultiplexing (U-OFDM) for OpticalWireless. In: Proc. of the Vehicular Technology Conference (VTC Spring), IEEE, IEEE, Yokohama, Japan
8. Tsonev D, Sinanovic S, Haas H (2013) Complete Modeling of Nonlinear Distortion in OFDM-based Optical Wireless Communication. J Lightw Technol 31(18):3064–3076,doi: 10.1109/JLT.2013.2278675
9. Asadzadeh K, Dabbo A, Hranilovic S (2011) Receiver Design for Asymmetrically Clipped Optical OFDM. In: GLOBECOM Workshops (GC Wkshps), IEEE, Houston, TX, USA, pp 777–781, doi: 10.1109/GLOCOMW. 2011.6162559
10. Dimitrov S, Sinanovic S, Haas H (2011) A comparison of OFDM-based modulation schemes for OWC with clipping distortion. In: GLOBECOM Workshops (GC Wkshps), 2011 IEEE, pp 787–791, doi: 10.1109/GLOCOMW. 2011.6162562
11. Dissanayake S, Panta K, Armstrong J (2011)A Novel Technique to Simultaneously Transmit ACO-OFDM and DCO-OFDM in IM/DD Systems. In: IEEE GLOBECOM Workshops (GC Wkshps), IEEE, Houston, TX, USA, pp 782– 786, doi: 10.1109/GLOCOMW.2011.6162561

12. Tsonev D, Videv S, Haas H (2015) Unlocking Spectral Efficiency in Intensity Modulation and Direct Detection Systems. IEEE J Sel Areas Commun PP(99):1–1, doi: 10.1109/JSAC.2015.2432530
13. Tsonev D, Sinanovic S, Haas H (2011) Enhanced Subcarrier Index Modulation (SIM) OFDM. In: GLOBECOM Workshops (GC Wkshps), IEEE, IEEE, Houston, Texas, USA
14. Dimitrov S, Sinanovic S, Haas H (2012)ClippingNoise in OFDM-Based OpticalWireless Communication Systems. IEEE Transactions on Communications 60(4):1072–1081, doi: 10.1109/TCOMM.2012.022712.100493
15. Dardari D, Tralli V, Vaccari A (2000) A Theoretical Characterization of Nonlinear Distortion Effects in OFDM Systems. IEEE Transactions on Communications 48(10):1755–1764,doi: 10.1109/26.871400
16. Proakis JG (2000) Digital Communications, 4th edn. McGrawHill, New York, NY, USA
17. Dimitrov S, Sinanovic S, Haas H (2012) Signal Shaping and Modulation for Optical Wireless Communication. Lightwave Technology, Journal of 30(9):1319–1328, doi: 10.1109/JLT.2012.2188376
18. Armstrong J, Schmidt BJC (2008) Comparison of Asymmetrically Clipped Optical OFDMand DC-Biased Optical OFDMin AWGN. IEEE Commun Lett 12(5):343–345, doi: 10.1109/LCOMM.2008.080193
19. Rajbhandari S, Chun H, Faulkner G, Cameron K, Jalajakumari A, Henderson R, Tsonev D, Ijaz M, Chen Z, Haas H, Xie E, McKendry J, Herrnsdorf J, Gu E, Dawson M, O Brien D (2015) High-speed integrated visible light communication system: Device constraints and design considerations. Selected Areas in Communications, IEEE Journal on PP(99):1–1, doi: 10.1109/JSAC.2015.2432551
20. ITU-T (2004) Forward Error Correction for High Bit rate DWDM Submarine Systems. Tech. Rep. ITU-T G.975.1, ITU
21. Dimitrov S, Haas H (2013) Information Rate of OFDM-Based Optical Wireless Communication Systems With Nonlinear Distortion. IEEE J Lightw Technol 31(6):918–929, doi: 10.1109/JLT.2012.2236642
22. Islim M, Tsonev D, Haas H (2015) A Generalized Solution to the Spectral Efficiency Loss in Unipolar Optical OFDM-based Systems. In: Proc. of the International Conference on Communications (ICC), IEEE, London, UK
23. Islim M, Tsonev D, Haas H (2015) On the Superposition Modulation for OFDM-based Optical Wireless Communication. In: Signal and Information Processing (GlobalSIP), 2015 IEEE Global Conference on, IEEE, Orlando, USA
24. Islim M, Tsonev D, Haas H (2015) Spectrally Enhanced PAM-DMT for IM/DD Optical Wireless Communications. In: Proc. of the 25th Int. Symp. Pers. Indoor andMobile Radio Commun. (PIMRC), IEEE, Hong Kong, China, pp 927–932